JOURNAL OF GEOPHYSICAL RESEARCH, VOL. 105, NO. B9, PAGES 21,333–21,352, SEPTEMBER 10, 2000

Integrated geological and geophysical studies in the SG4 borehole area, Tagil Volcanic Arc, Middle Urals: Location of seismic reflectors and source of the reflectivity

P. Ayarza,[1,2] C. Juhlin,[1] D. Brown,[3] M. Beckholmen,[1] G. Kimbell,[4] R. Pechnig,[5] L. Pevzner,[6] R. Pevzner,[6] C. Ayala,[4] M. Bliznetsov,[7] A. Glushkov,[8] and A. Rybalka[7]

Abstract. Near-vertical incidence reflection seismic data acquired in the Tagil Volcanic Arc (Middle Urals) show the upper crust to be highly reflective. Two intersecting seismic lines located near the ongoing ~5400 m deep SG4 borehole show that the main reflectivity strikes approximately N-S and dips ~35°-55° to the east. Prominent reflections intercept the borehole at ~1000, ~1500, 2800-2900, ~3400, and between ~4000 and 5400 m, which correspond to intervals of low velocity/low density/low resistivity. The surface projections of these reflections lie parallel to the strike of magnetic anomaly trends. Multioffset vertical seismic profile (VSP) data acquired in the SG4 borehole show a seismic response dominated by *P* to *S* reflected converted waves from the moderately east dipping reflectivity and from a set of very steep east dipping reflectors not imaged by the surface data. Modeling of the VSP data constrains the depth at which reflectors intercept the borehole and suggests that the *P* to *S* conversions are best explained by low-velocity porous intervals rather than higher-velocity mafic material. The most prominent east dipping reflection on the surface seismic data is only imaged on VSP shots that sample the crust closer to the E-W seismic line. This discrepancy between the VSP and the surface seismic data is attributed to rapid lateral changes in the physical properties of the reflector. Surface and borehole data suggest that the low-velocity/low-density/low-resistivity intervals are the most important source of reflectivity in the SG4 borehole area, although lithological contrasts may also play a role. Drill cores from the these zones contain hydrothermal alteration minerals indicating interaction with fluids. Tectonic criteria suggest that they might represent imbricated fracture zones often bounding different lithologies and/or intrusions. Some of them might also represent high-porosity lava flows or pyroclastic units, common in island arc environments.

1. Introduction

Reflection seismic studies have contributed greatly to our understanding of the structure of the Earth's crust. However, one common problem when interpreting these studies is determining the source of the reflectivity. Borehole data are the meeting point between geophysics and geology and their integration with reflection seismic data is necessary to constrain the source of the reflectivity in poorly exposed areas. Direct observations by borehole logging and probing and vertical seismic profile (VSP) studies have shown that open fluid-filled fracture zones (Manitoba, Canada [*Green and Mair*, 1983] and KTB (German Continental Drilling Program) [*Lüschen et al.*, 1996; *Harjes et al.*, 1997]), mylonitc zones (Brevard Fault Zone [*Christensen and Szymansky*, 1988]), dolerite sills (Siljan Ring [*Juhlin*, 1990]), metasedimentary lithologies (Sudbury Basin [*Miao et al.*, 1994]), and compositional boundaries plus faults and fluid-filled fractures (SG3 [*Pavlenkova*, 1992; *Ganchin et al.*, 1998]) have a major effect on crustal reflectivity.

Extensive surface seismic studies carried out in the Middle Urals (Figure 1) have shown the upper crust to be highly reflective [*Juhlin et al.*, 1995, 1997, 1998; *Steer et al.*, 1995]. Prominent reflectors have been penetrated by the SG4 borehole and have been locally interpreted as fracture zones, possibly related to lithological contacts [*Juhlin et al.*, 1997]. However, reflection seismic profiling over the Magnitogorsk Volcanic Arc, the equivalent unit of the Tagil Volcanic Arc in the Southern Urals, shows weaker reflectivity in the upper crust [*Brown et al.*, 1998; *Echtler et al.*, 1996]. In the modern Banda Arc the upper crust is only weakly reflective [*Snyder et al.*, 1996]. The internal architecture of volcanic arcs is complex, with rapid changes in stratigraphic thickness and composition making it difficult to link reflectivity to any one of the causes listed above. It is therefore of interest to accurately locate the reflectors in the Tagil Volcanic Arc area by linking them to direct observations in the SG4 borehole. With this goal in mind, a multidisciplinary study has been carried out in the SG4 borehole area in the Middle Urals. Two surface seismic lines crossing near the SG4 borehole (ESRU95, Figure 1) are used to determine the strike and dip of

[1]Department of Earth Sciences, Uppsala University, Uppsala, Sweden.
[2]Now at Departamento de Geología, Area Geodinámica, Universidad de Salamanca, Salamanca, Spain.
[3]Instituto de Ciencias de la Tierra 'Jaume Almera,' Consejo Superior de Investigaciones Científicas, Barcelona, Spain.
[4]Regional Geophysics Group, British Geological Survey, Keyworth, Nottingham, England, United Kingdom.
[5]Applied Geophysics, Aachen University of Technology, Aachen, Germany.
[6]Nedra, Yaroslavl, Russia.
[7]Bazhenov Geophysical Expedition, UralGeolKom, Scheelit, Russia.
[8]UralGeolKom, Urals Geological Survey Expedition, Ekaterinburg, Russia.

Paper number 2000JB900137.
0148-0227/00/2000JB900137$09.00

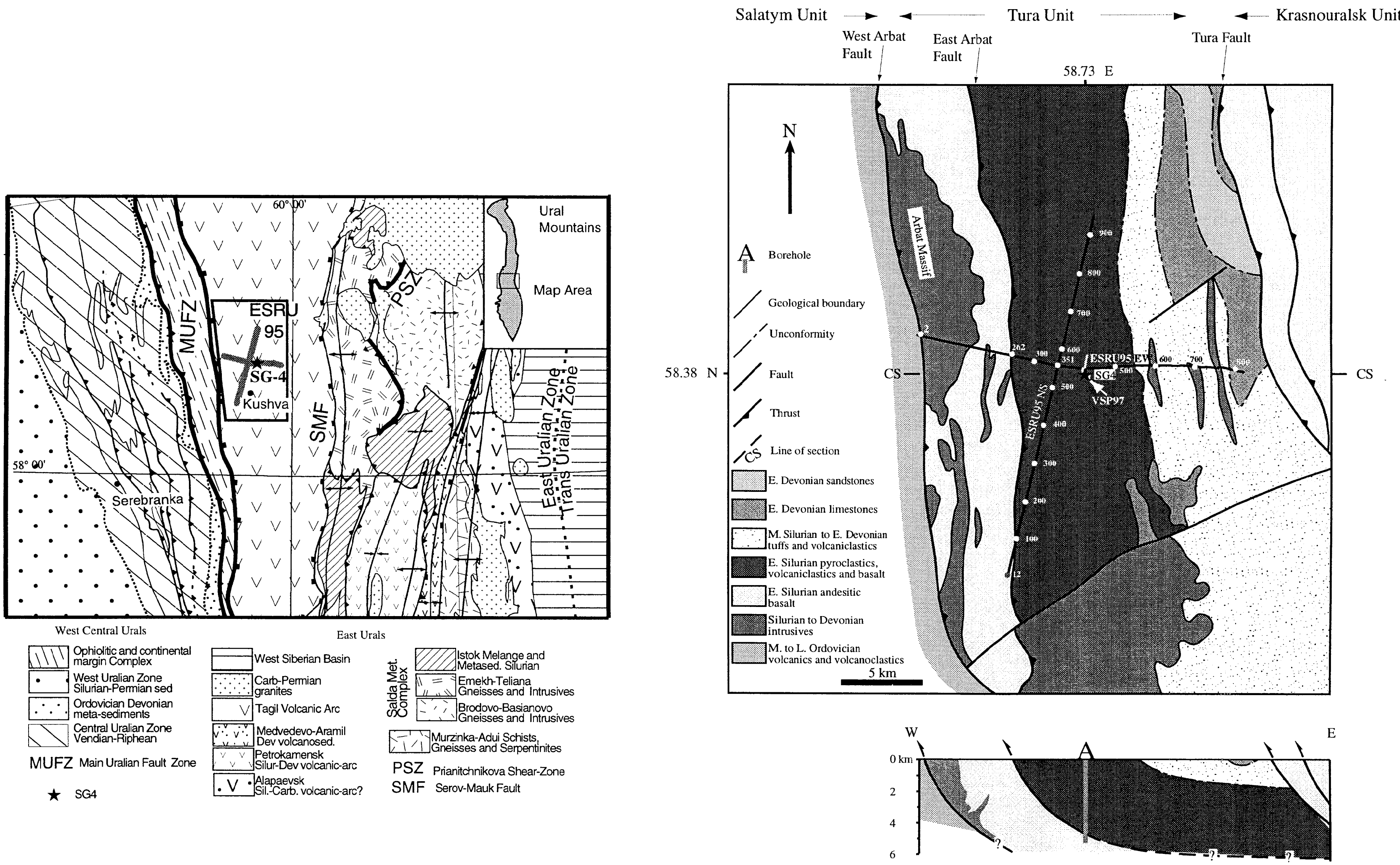

a) b)

Figure 1. (a) Geological map of the Middle Urals [after *Juhlin et al.* 1998] with the location of the ESRU95 seismic line. (b) Geological map of the Middle Urals in the SG4 vicinity (area enclosed in the box in Figure 1a) and simplified cross section of the same area. The location of the ESRU95 lines and that of the new VSP97 experiment is indicated.

the reflectivity. Migration of a section perpendicular to the approximate strike of the reflectors gives information about their dip and the depth at which they intercept the borehole. Core data are used to study the physical properties of the rocks where the reflectors intercept the borehole. Processing and modeling of VSP (VSP94 and VSP97, Figure 1 and Plate 1) data are used to further constrain the exact location of the reflectors and the source of the reflectivity.

2. Geological Background

The Paleozoic Uralide Orogen formed as a result of the accretion of island arc complexes to the East European Craton (EEC) along an east dipping subduction zone marked by the Main Uralian Fault Zone (MUFZ) during the Late Devonian to Early Carboniferous, followed by closure of the Paleo-Uralian ocean and collision of the amalgamated Asian continent. Subsequently, a foreland thrust and fold belt and foreland basin developed in the Southern and Middle Urals from the Late Carboniferous to Early Triassic. To the east of the MUFZ in the Southern Urals, the crustal structure and timing of the accretion of the Magnitogorsk Arc are well constrained [e.g., *Brown et al.*, 1998]. In the Middle Urals (Figure 1a), however, the timing of accretion of the Tagil Arc and its resultant structure are less well understood due to poor exposure and to the absence of collision-related, arc-derived sediments overlying the former platform margin. It is thought, however, that the Tagil Arc had accreted by the Early Carboniferous (Visean) [e.g., *Zhivkovich and Chekhovich*, 1986; *Puchkov*, 1997]. In the Late Carboniferous-Early Permian, sinistral strike-slip faulting affected the Middle Urals, and thus the Tagil Arc [*Ayarza et al.*, 2000]. *Knapp et al.* [1998] suggest that it was also affected by post-orogenic extension in Early Mesozoic times.

The Tagil Arc (Figure 1) consists predominantly of Ordovician to Silurian age andesitic to dacitic basalts of island arc affinity and Silurian to Lower Devonian arc-derived pyroclastics and volcaniclastic sediments, unconformably overlain by Early to Middle Devonian shallow water carbonates. It is bounded to the west by the east dipping MUFZ and to the east by the steeply west dipping Serov-Mauk Fault [*Steer et al.*, 1995; *Juhlin et al.*, 1998; *Friberg and Petrov*, 1998]. The Tagil Arc can be divided, from west to east, into three different units: the Salatym Unit, the Tura Unit, and the Krasnouralsk Unit (Figure 1b) which represent various stages of the arc building process. The SG4 borehole and the surface seismic data discussed in this paper are within the Tura Unit, which is composed of Early Silurian basalts and dolerites and plagiorhyolites of island arc-related chemistry, representing the first stages of the arc buildup. In the western part the Tura Unit is intruded by dunite-clinopyroxenites, gabbros, and plagiogranites of the Arbat Massif, which belong to the platinum-bearing belt. In the eastern part, up to 5000 m of pyroclastic and volcaniclastic units imbricated by east dipping thrusts are present. The Arbat Massif is bounded to the west by the West Arbat Fault and to the east by the East Arbat Fault. Farther to the east, the Tura Unit is bounded by the east dipping Tura Fault. Most of these features have a distinct aeromagnetic signature and, owing to the poor exposure of the area, have been largely mapped using aeromagnetics (Plate 1) and other geophysical methods.

3. SG4 Borehole

In June 1985 the Soviet Deep Drilling Program began drilling the SG4 borehole in the western part of the Tagil Arc (Figure 1 and Plate 1) with the objectives to study the tectonic history of the area, its mineral resource potential, and the nature of seismic reflections. By August 1995 it had reached 5345 m when drilling stopped. The work was later resumed, and by June 1999 it had reached 5401 m. The current Russian government plans to deepen the current borehole down to 8000 m and then case it. If this stage is successful, the borehole will then continue to be drilled to the targeted depth of 15,000 m. The drilling equipment, Uralmash 15000, performs continuous core extraction and has had an average recovery rate of 64%. At the time of the VSP surveys discussed in this paper the borehole consisted of two holes (Figure 2): a small diameter pilot hole, which deviates slightly to the northeast, drilled to 3975 m and a larger diameter main hole, which deviates to the southeast down to 4600 m and to the southwest from 4600 m on. The pilot hole has been cored and logged. The main hole has been logged in its entirety and cored below 4000 m. The effect of the deviation of the two holes will be considered below. The following is a summary of the core description.

The upper 430 m of the borehole (Figure 3a) are dominated by basaltic and andesitic lavas, pillow lavas, and hyaloclastic flows. From 430 to ~3050 m the lithology consists of pyroclastic flows, locally intruded by dolerite and diorite dikes. From the core description, individual pyroclastic flows cannot be identified with confidence. Alteration to epidote, prehnite, chlorite, and carbonate is widespread in and around fractures. Sulfide impregnations are found in discrete intervals. From ~3050 to ~4650 m, thin- to thick-bedded volcaniclastic sandstones to conglomerates interbedded with carbonaceous and siliceous siltstones are found. Local intercalations of pyroclastic agglomerates and tuffs and rare andesitic lava flows also exist. Sediment clasts are mostly andesitic to dacitic in composition from ~3000 to ~3500 m. Between ~3500 and ~4300 m the sedimentary input is higher. In the interval ~3500-4650 m, fracturing and intrusions of dioritic to gabbroic dikes are widespread. Alteration to epidote, prehnite, chlorite, and carbonate is common, with local occurrences of sulfide mineralization. Between ~4650 and ~5175 m, intercalated andesitic basalts, pyroclastic flows, and volcaniclastic sediments, all extensively intruded by thin dikes of variable composition (dolerite, diorite, melanobasalt, etc.) are observed. From ~5175 m to the end of the core log at 5354 m, the rocks consist of extensively fractured and locally metasomatised basaltic, andesitic, and dacitic lava flows. Poor exposure and rapid lateral lithological changes common in arc environments hinder a straightforward correlation between lithologies found in the borehole and those interpreted on the geological map. The lithologies found in the borehole (which belong to the Tura Unit) are significantly thicker than expected from surface geology [*Bashta et al.*, 1996; *Karetin*, 1992].

4. Borehole Geophysics

Bulk density, specific electrical resistivity, magnetic susceptibility, V_p, and V_s were measured over decimeter to meter intervals in wet samples at room temperature and pressure. In situ physical properties (density, V_p, resistivity, magnetic susceptibility, natural gamma, neutron porosity) were recorded by downhole measurements at 0.2-m intervals. However, the wire line log data set has not been made available in its entirety. In addition, its quality is highly influenced by breakout zones, which occur frequently in the deeper part of the hole. The large diameter and the rugosity of the borehole wall cause unrealistic values of density, V_p, and V_s. Thus wire line logging data are only

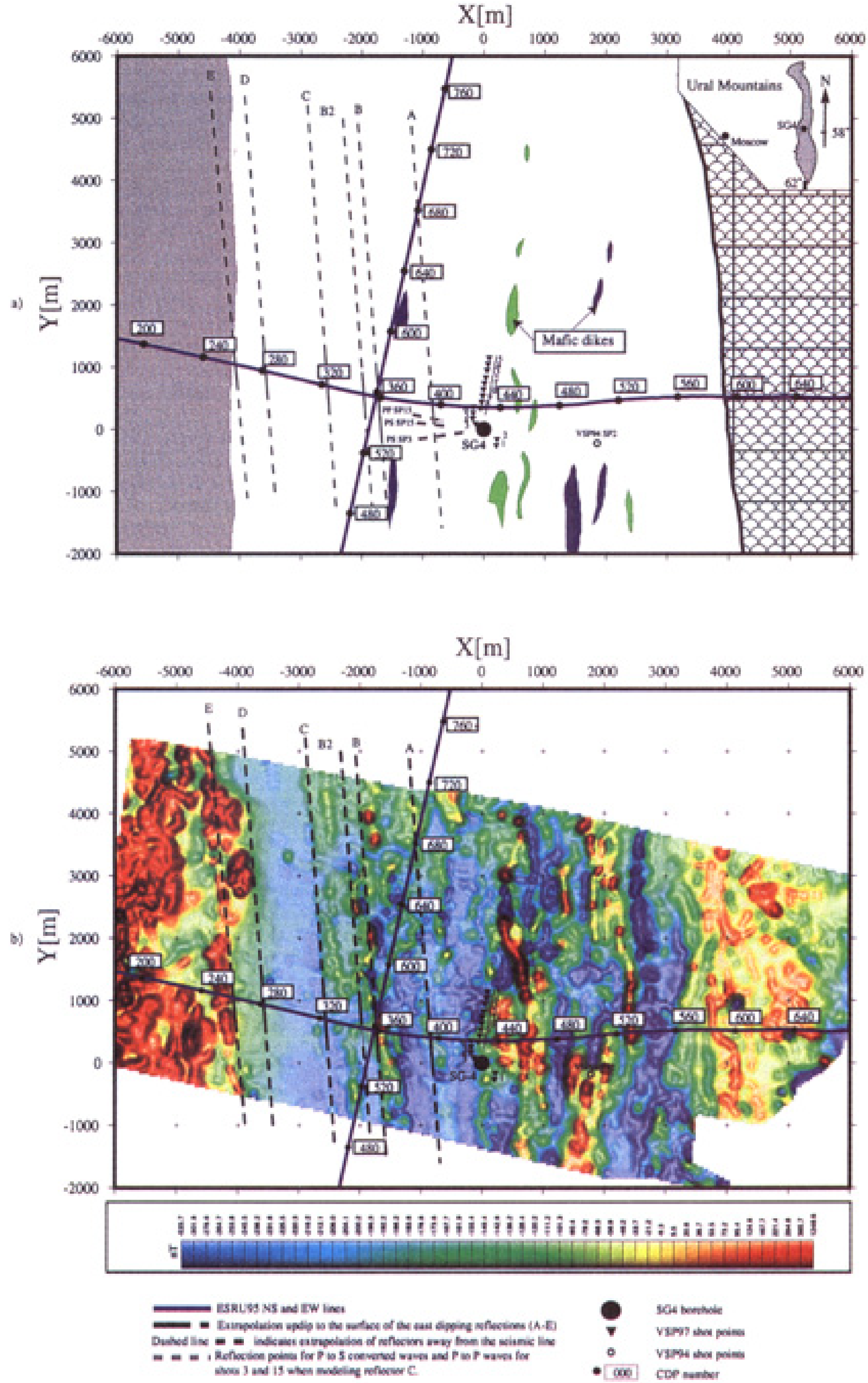
a)
X[m]
Y[m]
Ural Mountains
N
Moscow
SG4
58°
62°
Mafic dikes
SG4
E
D
C
B2
B
A
b)
X[m]
Y[m]
ESRU95 NS and EW lines
Extrapolation updip to the surface of the east dipping reflections (A-E)
Dashed line indicates extrapolation of reflectors away from the seismic line
Reflection points for P to S converted waves and P to P waves for shots 3 and 15 when modelling reflector C.
SG4 borehole
VSP97 shot points
VSP94 shot points
CDP number

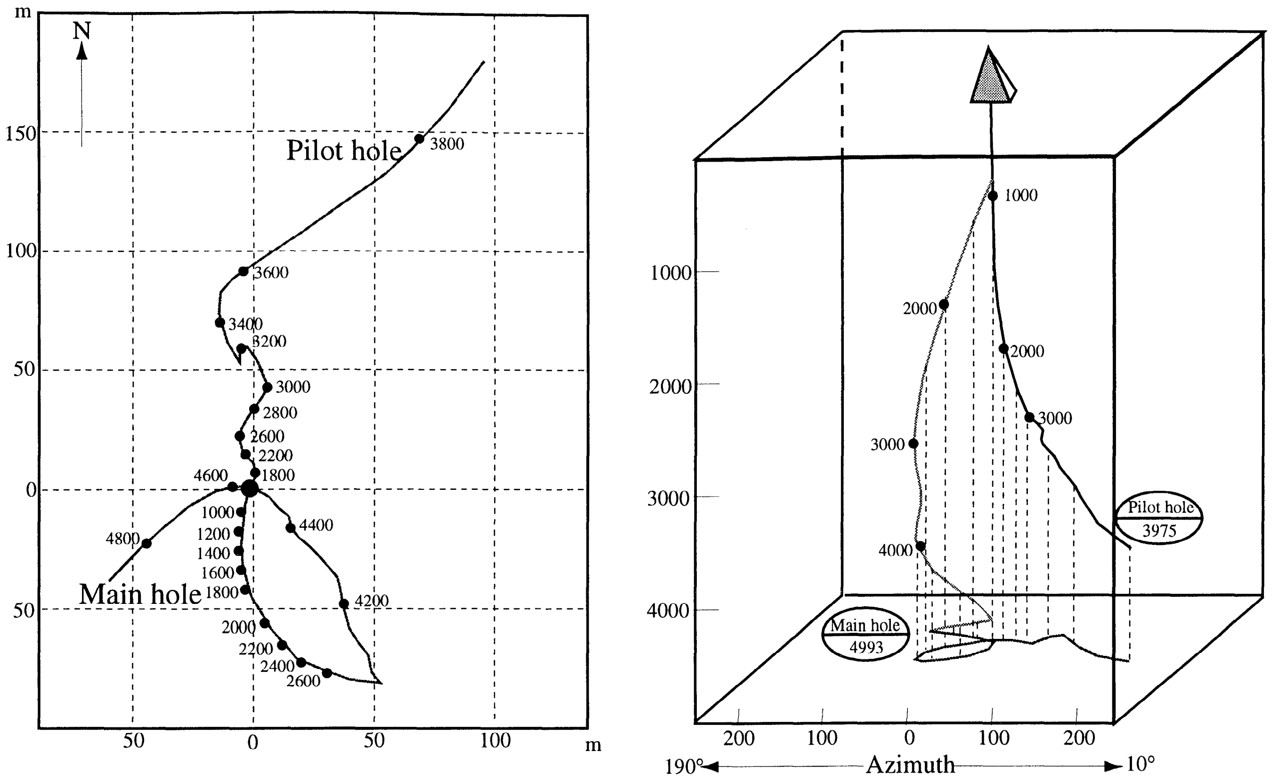

Figure 2. Drilling trajectory of the pilot and main SG4 holes at depth. Distances and depth are in meters.

used in this paper when explicitly stated. Core values from the pilot hole, averaged to 10-m intervals, plus an interval (1450-1550 m) of the wire line logging data are shown in Figure 3a.

Core density data ranges between 2.69 and 2.96 g/cm^3 (Figure 3a). The average density for the near-surface lavas and the upper part of the pyroclastic sequence (down to ~2400 m) is ~2.82 g/cm^3 (Figure 3a). Higher densities occur in the lower part of the pyroclastic unit and coincide with higher magnetic susceptibilities. In the underlying volcaniclastic rocks the density decreases sharply from 2.82 g/cm^3 to 2.76 g/cm^3 below 3400 m. The heterogeneous sequence in the interval 4650-5175 m has widely varying densities, whereas the lava flows below 5175 m are characterized by high densities and magnetic susceptibilities. The density histogram (Figure 4a) shows a main peak at 2.82-2.83 g/cm^3 and a secondary peak at ~2.74 g/cm^3. The tail at higher densities reflects high values found at 1460-1490 m (2.9-2.92 g/cm^3), 2430-2500 m (2.91-2.96 g/cm^3), 2790-2840 m (2.9-2.92 g/cm^3), and 5130-5260 m (2.9-2.94 g/cm^3). There is no systematic increase of the core densities with depth and low values appear deep in the borehole. Core density data must, however, be treated with caution because of the decompression effects caused by bringing deep samples to the surface.

V_p values (Figure 3a) have an asymmetric distribution (Figure 4a) showing a median of 6.18 km/s with a tail toward lower velocities. The highest V_p values are found between 2250 and 2500 m (6.53 and 6.66 km/s) where they locally coincide with high densities and high magnetic susceptibilities (709-932 x10^{-5} SI units). Low V_p zones appear at ~1000 m (V_p=3.25-4.57 m/s), ~2900-3000 m (V_p=4.34-5.37 km/s), ~3400-3500 m (V_p=4.59-5.61 km/s), ~3800-4000 m (V_p=4.1-5.3 km/s), and in the interval ~4000-5350 m (V_p=4.55-5.61 km/s). From 1440 to 1560 m, only wire line logging data exist, showing very low V_p values (3.5-4 km/s) in the interval 1480-1490 m (Figure 3a). In most cases, low-V_p zones also have low densities (e.g., ~3400, ~5000 m) and often bound high-density/high-magnetic susceptibility intervals (e.g., 1012 x 10^{-5} SI units at ~930 m, 657 x 10^{-5} SI units at 2800 m, 1894 x 10^{-5} SI units at 5260 m). The locations of the low-V_p zones in the SG4 borehole coincide with low interval velocities as calculated from the VSP97 data (Figure 3b) using the common excitation array (CEA) method [*Bliznetsov and Juhlin*, 1994] . From the density and V_p core data the P wave impedance may be calculated (Figure 3a). V_p has a greater impact than density on the impedance, and this observation will be considered further in the discussion.

Plate 1. (a) Simplified geological sketch of the SG4 area interpreted from aeromagnetic data (see Plate 1b and *Juhlin et al.* [1997]). Location of SG4 borehole, shot points for VSP experiments, surface seismic lines, and surface traces of reflectors identified on the surface seismic data in Plate 2 and Figure 5 are shown. Dashed lines show the extrapolation of the surface trace of the reflections away from the seismic line. Observe that reflection points obtained after modeling reflector C for shot 15 (VSP97) lie closer to the ESRU95 E-W seismic line than those for shot 3. (b) Magnetic map of the SG4 area plotted as a shaded relief image using equal color area and vertical illumination. Total magnetic field data collected along ground traverses ~100 m apart. Location of SG4 borehole, shot points for VSP experiments, surface seismic lines, and surface traces of reflectors identified on the surface seismic data in Plate 2 and Figure 5 are shown.

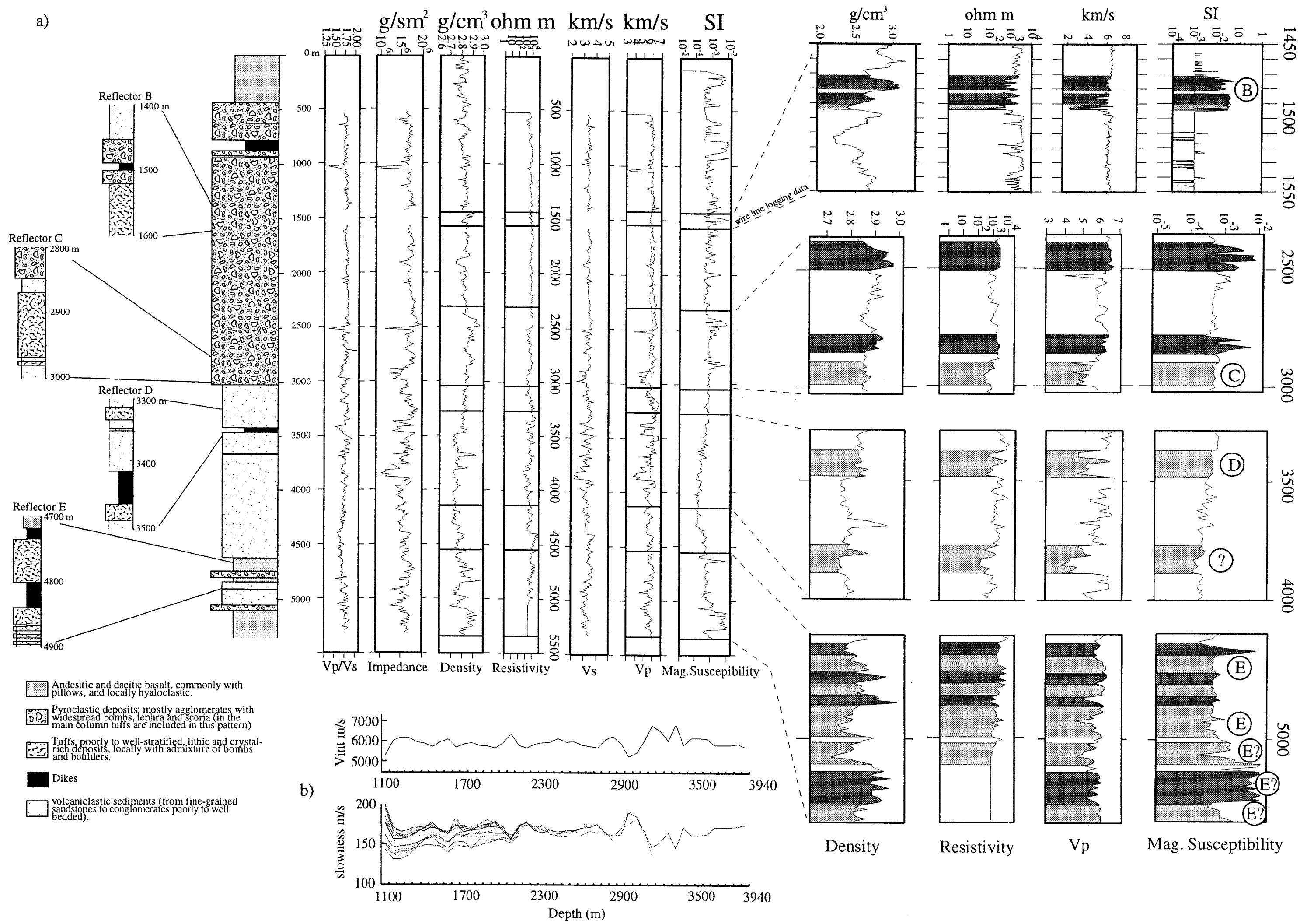

Figure 3. (a) Core data from the SG4 borehole and stratigraphic column of the borehole. Details of potentially reflective intervals are shown on the right. Detailed interval between 1400 m and 1600 m corresponds to wireline logging data. Dark shading indicates potential basic intercalations. Light shading indicates zones of likely higher porosity. Impedance calculated from V_p and density core data and V_p/V_s ratio are also shown. Observe that the pattern followed by the impedance is close to that followed by V_p. (b) Slowness and V_p interval velocity as calculated from the common excitaton array (CEA) method [*Blitznetsov and Juhlin*, 1994] over the VSP97 data. For comparison purposes, V_p interval velocity from VSP97 is also plotted on V_p core data frame.

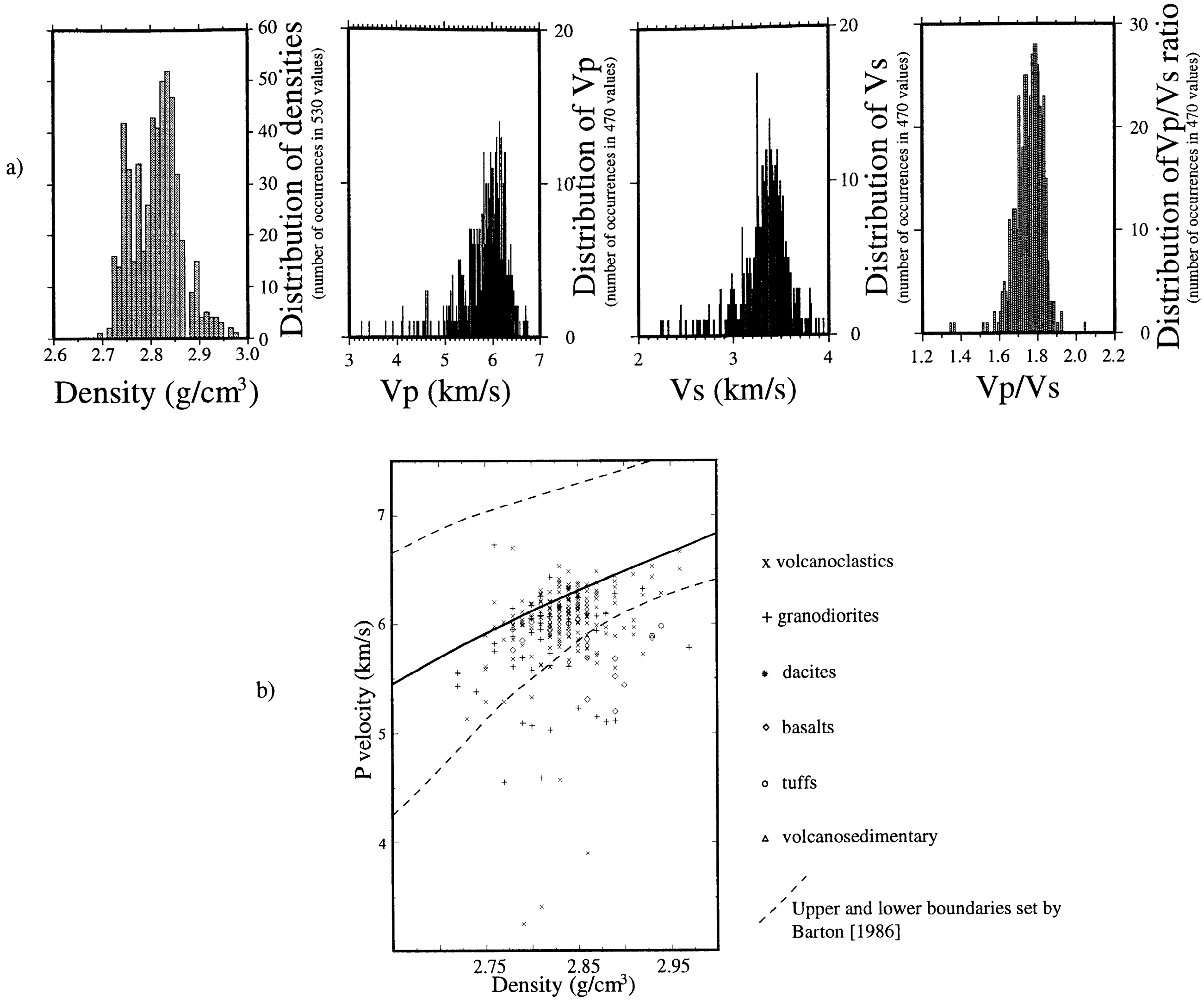

Figure 4. (a) Histograms of the distribution of density, V_p, V_s and V_p/V_s. (b) V_p-density cross plot in relation to the empirical relationships described by *Barton* [1986]. Solid curve represents the general relationship between V_p and density, and dashed curves represent the upper and lower velocity bounds given by *Barton* [1986].

V_s shows a distribution similar to that of V_p (Figures 3a and 4a). The median is 3.4 km/s, although there is a narrow peak at 3.25 km/s. Very low V_s values (<3 km/s) appear deep in the borehole (Figure 3a), at ~2900-3000, ~3400-3500, ~3800-4000, and ~4000-5350 m (mostly between 4900 and 5250 m). No V_s values exist from the low V_p intervals at ~1000 and ~1500 m. The V_p/V_s ratio (Figure 3a) shows a Gaussian distribution (Figure 4a) of values that mainly range between 1.6 and 1.9. Lower (1.35) and higher (2.04) values appear locally. There is no systematic increase of V_p/V_s with depth, and low V_p/V_s values (<1.7) appear in the borehole below ~2900 m.

Low resistivity values are found at ~2900 m (1200-2600 ohm m) and ~3400 m (1150-4000 ohm m) (Figure 3a). The most striking low-resistivity zone is at ~3850 m, where values drop by almost 3 orders of magnitude. In these three intervals, V_p and V_s are low. The interval between 4000 and 5060 m (no values were measured deeper than 5060 m) shows highly variable resistivities with low values in some intervals (e.g., 1500 ohm m at 4360 m and 2400 ohm m at 4830 m) and very high values in other intervals (e.g., 83000 ohm m at 4410 m and 32000 ohm m at 4760 m).

5. Interpretation of Borehole Geophysical Data

Core density data often show a relationship with other physical properties that allows us to interpret lithologies. High densities occur along the entire borehole and often coincide with high magnetic susceptibilities and high V_p (e.g., ~2500 m), suggesting an association with more basic flows and/or intrusions. Often, intervals of high densities are bounded by narrow low V_p-low-density zones (e.g., ~1000, ~1500, ~2500 m). Core descriptions indicate that at ~1000 and ~1500 m there are diabase and diorite dikes. They are probably associated with fracture zones. A decrease in density below 3000 m associated with low V_p (e.g., ~3400 and ~3900 m) may correspond to an increase in the content of silicic and carbonate sediments and/or to an increase in porosity. Often, low density and low V_p values are associated with low resistivities (e.g., ~2900, ~3900, and locally between ~4000 and 5250 m), which suggests that we might be looking at fluid-filled or sulfide-impregnated porous intervals. Typical minerals found in these intervals are hydrothermal alteration products such as epidote, calcite, chlorite, and prehnite. Sulfides, however, do not appear in thick high-porosity zones but do appear in very thin intervals.

Distributions of V_p similar to that of the SG4 borehole have been widely attributed to zones of fracturing (secondary porosity) [*Holliger et al.*, 1996; *Lüschen et al.*, 1996; *Frenje and Juhlin*, 1998]. Low V_p values could also be related to intervals of higher primary porosity common to volcanic lithologies. A complicating factor is that V_p measurements from deep boreholes made on cores at low confining pressures might reflect the effect of stress relief [*Vernik et al.*, 1994]. Drilling- and coring-induced microcracks may significantly reduce the measured velocities on core when compared to the in situ velocities, especially below depths of 4 km [*Vernik et al.,* 1994]. Core data may also contain some sampling bias since measurements will preferentially be made on intact cores rather than on highly fractured sections. For the present data set the core velocities are generally low where existing sonic velocities are also low [*Juhlin et al.*, 1997] and broadly coincide with those calculated from the VSP97 data (Figure 3b). Thus we consider the core values to reflect real physical properties of the rocks at depth.

Core data suggest that the SG4 borehole is located in an area where either primary or secondary porosity is high and intrusions are common, especially below ~2900 m. Six prominent low-velocity/low-density/low-resistivity (LVDR) zones have been interpreted to be present in the borehole at ~1000, ~1500, ~2900, ~3400-3500, and ~3800 m, and within the interval ~4000-5250 m. A V_p-density cross plot (Figure 4b) shows a large scatter for V_p and a tendency for V_p values to be lower for a given density than is typically observed [e.g., *Nafe and Drake*, 1957; *Ludwig et al.*, 1970; *Barton,* 1986]. The relationship between velocity and density is only a general one, so some difference between the pattern observed in the arc-related rocks from the SG4 area and an average based primarily on different lithologies is not surprising. However, the cross plot contains a significant population of points which lie well outside the lower-velocity bound set by *Barton* [1986]. These are not confined to a particular rock type and are interpreted as the effect of fracturing or primary porosity, which influences V_p far more than density. The thickness of the fracture zones as deduced from the core anomalies is of the order of 100-200 m in the borehole direction below 2900 m. The zones at ~1000 and ~1500 m, associated with diorite and dolerite intrusions, are, however, considerably thinner.

6. Reflection Seismic Data, ESRU95

Two crossing surface seismic reflection profiles were acquired over the SG4 borehole during winter 1994/1995 as part of the Europrobe´s Seismic Reflection Profiling in the Urals (ESRU) program (ESRU95 N-S and E-W, Figure 1 and Plate 1). A crustal-scale interpretation of the E-W line has been previously presented by *Juhlin et al.* [1998], and a more detailed one near the SG4 borehole has been presented by *Juhlin et al.* [1997]. Here we present a regional joint interpretation of both lines (Plate 2) with the aim to identify the strike and dip of the main reflectivity. This will then later be integrated with the other data sets to determine the source of the reflectivity. The processing presented here uses higher stacking velocities than those used by *Juhlin et al.* [1997], and thus steeply dipping events are imaged better. This is important since conventional processing of two-dimensional (2-D) seismic data enhances subhorizontal reflectivity, resulting in misleading interpretations in areas with steeply dipping reflectors [*Harjes et al.*, 1997]. Acquisition parameters are given by *Juhlin et al.* [1998], and the processing steps are given in Table 1.

On the E-W line (Plate 2), a set of strong east dipping events appears to correspond to a set of gently north dipping events interpreted on the N-S line. The integrated interpretation of the two (Plate 2) allows us to subdivide this reflectivity into five groups of reflectors, labeled A, B, C, D, and E, with event C being the strongest. They strike at ~N355°. Their surface traces are nearly parallel and are oriented along the same trend as the magnetic anomaly pattern (Plate 1b). Reflectors A and B project to the surface within a pyroclastic unit, along ~N-S lines previously interpreted as fault zones on the basis of magnetic data [e.g., *Juhlin et al.*, 1997]. C projects along the ~N-S lithological boundary between the pyroclastic sequence and the (nonmagnetic) volcaniclastic unit, which has been interpreted as a fault and/or thrust-related contact [*Juhlin et al.*, 1997]. D projects between a volcaniclastic unit and underlying magnetic lavas, close to E, which projects along the East Arbat Fault. In the E-W line, two other reflectors, F and G (Plate 2), appear to project to the surface within the Arbat Massif (F) and at the westernmost geological feature imaged by the ESRU95 E-W line, the West Arbat Fault (G), which also defines a lithological boundary (Plate 1a).

A recent seismic study in an Archean terrane in Canada shows that sideswipes from near vertical dolerite dikes can generate seismic reflections that can be misinterpreted as originating from gently dipping interfaces below the seismic profile [*Zalewski et al.*, 1997]. The presence of dolerite and dolerite dikes in the SG4 borehole and the linear magnetic highs in the area indicate that this possibility should also be considered for reflectors A-E. However, the subhorizontal nature of the reflectivity on the ESRU95 N-S line and the apparent dip of ~45° on the ESRU95 E-W line rules out the possibility that the reflectors originate within the near surface from near vertical structures.

A weaker set of west dipping reflections observed in the ESRU95 E-W line (Z in Plate 2) could be related to a set of weak, discontinuous south dipping reflections in the ESRU95 N-S line. The existence of these reflections is clear in shot gathers [see *Juhlin et al.*, 1997, Figure 10]. Their interpretation, however, remains unclear on the stacked sections and they will not be discussed in this paper.

Since east dipping reflections (events A-E) originate from nearly within the plane of the E-W profile, they will migrate approximately to their correct spatial position. Accordingly, the upper 4 s of the ESRU95 E-W line have been migrated and depth converted (Table 1 and Figure 5) in order to establish correlations between reflectivity and the borehole data. The section obtained here differs from that of *Juhlin et al.* [1997] in that (1) we have not applied dip move out (DMO) and (2) migration velocities have been taken from the VSP94 velocities [*Juhlin et al.*, 1997]. In spite of not applying DMO, zones with opposite dips are well resolved (Figure 5), probably due to the higher stacking velocities and more accurate migration velocities.

The migrated section in Figure 5 shows that (1) reflectors A-E are better defined and become listric after migration, showing dips of ~35°-50° at the surface, (2) reflector C shows two clearer branches, the upper one, listric, flattening to the east and the lower one dipping to the east and soling out (or getting crosscut) by the underlying reflector D to the east of the borehole at ~4300 m and (3) assuming no lateral variations in reflectivity along strike, reflectors A, B, C, and D project into the borehole at around 1000, 1400-1500, 2800-2900, and 3400-3500 m, respectively. The listric extension of E is a zone of reflectivity that projects into the borehole from ~4000 m to ~5400 m. F and

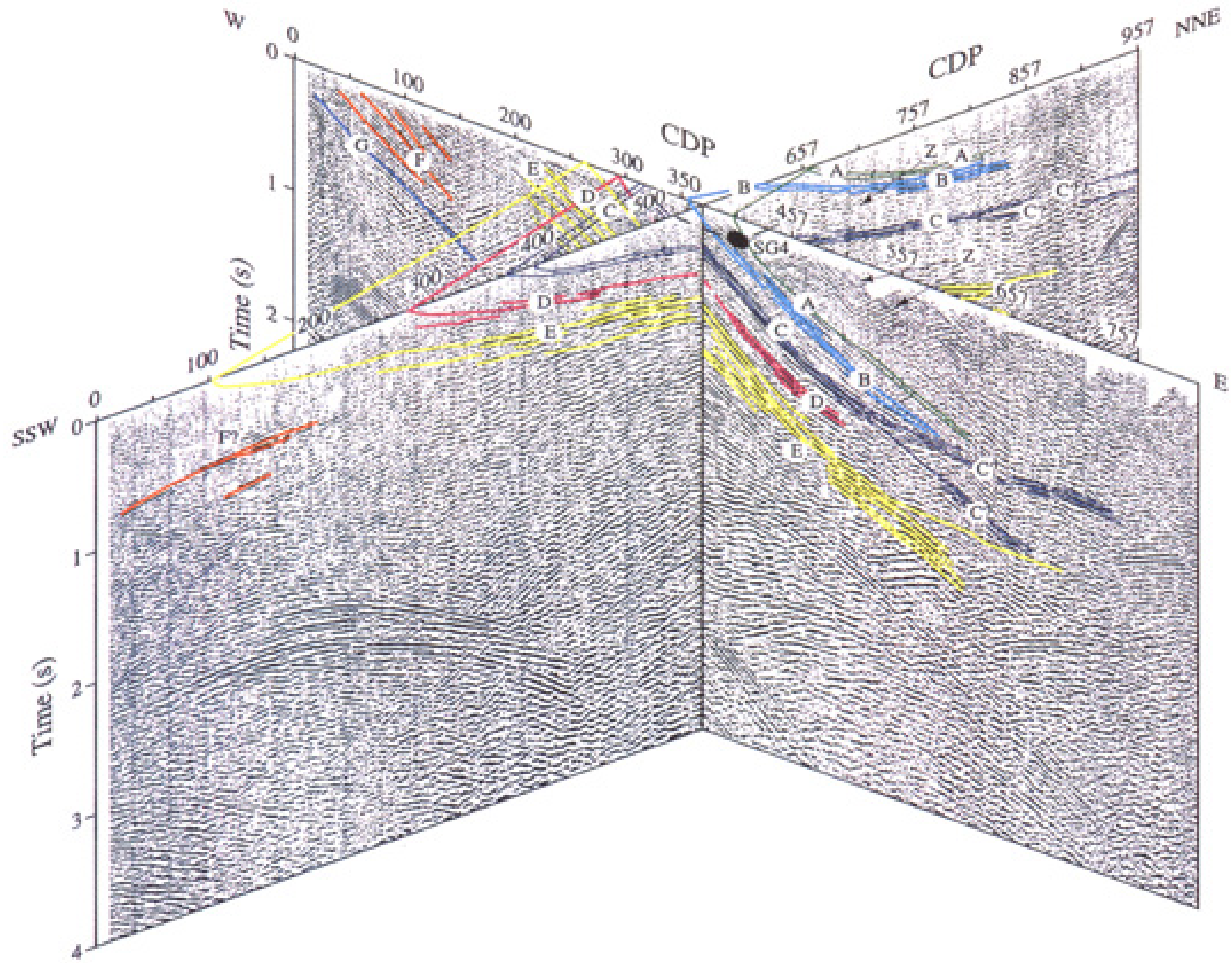

Plate 2. Composite section of the ESRU95 N-S and E-W seismic lines with an overall interpretation of the main reflections observed in the two lines and their correlation. Since some reflections reach the surface, their strike (~N-S) can be inferred. See Plate 1 for a view of the locations where these events outcrop. Distance between common depth points (CDPs) is 25 m.

Table 1. Processing Steps for ESRU95 Data

Step	Description
1	Read SEGY data
2	Input and apply geometry
3	Spherical divergence
4	Trace editing
5	Refraction statics
6	Automatic gain control (AGC), 100 ms window
7	Band-pass filter: 20-30-90-120 Hz (0-500ms), 15-22-80-120 Hz (400-2000 ms),10-20-60-75 Hz (1800-4000 ms)
8	Sort CDPs
9	Velocity analysis
10	Residual statics
11	Normal move-out (NMO)/stacking
12	Trace equalization
13	F-X deconvolution
14	Stolt *fk* migration; *v*=6.0 km/s (displayed in Figure 5)
15	Depth conversion (displayed in Figure 5)

G do not seem to be intersected by the borehole. Note also that a relatively clear event appears at ~2000 m on the migrated section (labeled B2 in Figure 5) that is not clearly seen on the stacked section. The surface trace of this event (labeled B2 in Plate 1b) is assumed to be parallel to the dominant ~N-S trending magnetic anomaly.

7. Multioffset Vertical Seismic Profiling (VSP97)

In order to further study the source of the reflectivity in the SG4 borehole area, an ~E-W oriented VSP experiment was acquired in August 1994 (VSP94, Plate 1). Interpretation of these data [*Juhlin et al.*, 1997] showed that the east dipping reflectivity correlated in part with fracture zones as interpreted from magnetic data, often subparallel to lithological boundaries. Many of the reflections, however, remained uncorrelated, and the most pronounced reflection on the ESRU95 line (C reflector) was not well imaged on the VSP94 data. Additional VSP data, oriented perpendicular to the VSP94 experiment, were acquired in March 1997 (VSP97, Plate 1) in an attempt to image reflector C laterally away from the borehole and to acquire additional information on the seismic properties of the upper crust of the Tagil Arc. Both experiments were carried out in the SG4 main hole (Figure 2). Acquisition steps for both experiments are shown in Table 2. Processing and interpretation of the VSP97 data as well as further processing of the VSP94 data are presented in sections 7.1 and 7.2.

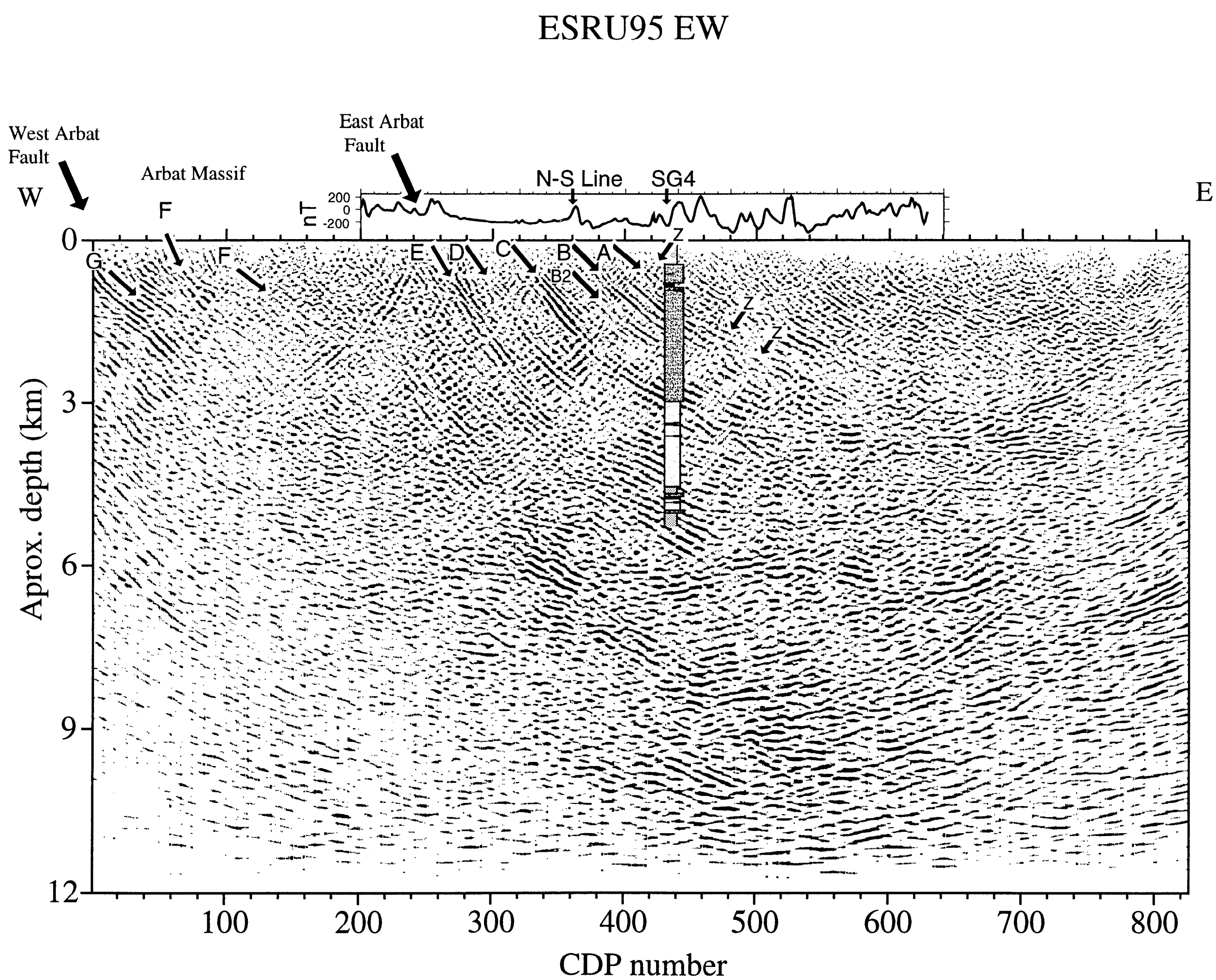

Figure 5. Migrated section of the reprocessed ESRU95 E-W line. A-G correspond to the studied set of east dipping reflections. Z represent weaker west dipping reflections. Observe the correlation between the surface projection of reflections A-G, mapped faults (Plate 1a) and the observed magnetic pattern (Plate 1b).

Table 2. Acquisition Parameters for the VSP97 and VSP94 Data

Parameter	VSP97	VSP94
Receiver probe	Three points, three components	one point, three components
Geophone type	14 Hz, SMC 14-1850	20 Hz, four component Galperin
Receiver probe spacing	60 m	20 m
Number of shots	368	344
Depth of shot holes	SP 1-6, 15 m	SP 1 (135 m offset), 9 m
Depth of shot holes	SP 7-15, 5 m	SP 2 (1835 m offset), 15 m
Charge	0.4 kg	SP 1, 0.5 kg. SP 2, 1 kg
Recording instrument	IBM PC	PROGRESS
Sample rate	1 ms	2 ms
Record length	3400 ms	5000 ms
Field low cut	Out	28 Hz
Field high cut	250 Hz	125 Hz

VSP 97 Shot	Top Depth, m	Bottom Depth, m	Range, m	Number of Shots
1	1120	2960	1800	31
2	1120	2960	1800	31
3	1120	2660	1500	26
4	1120	3200	2040	35
5	1120	3920	2760	47
6	1120	2300	1140	20
7	1120	3140	1980	34
8-15	1120	2180	1020	144

Total number of shots is 368

7.1. VSP97 Acquisition

Original plans to acquire data from 24 shot points to the north of the borehole at offsets ranging from 100 to 2400 m over a depth interval from 1000 to 3000 m had to be canceled due to logistics and severe weather conditions. Instead, only 15 shot points (Plate 1) could be used and were recorded over a depth interval starting at 1120 m and ending as shallow as 2180 m. Shots 1-7 were recorded down to deeper levels, extending as deep as 3920 m on shot 5 (Table 2). A three-component, three-unit tool with 20-m spacing between the units was used for the acquisition. The best quality data were acquired from shot points 3, 4, 5, and 7 (e.g., shot 3, Figure 6a). Data north of shot point 7 have a lower frequency content than those to the south (e.g., shot 12, Figure 6b) and a source ghost appears at ~130 ms after the first arrival. In all shots the data quality on the horizontal components is poorer than on the vertical component.

7.2. VSP97 Processing and Location of Seismic Reflectors in the Borehole

The horizontal component data used to orient the geophones provided a consistent coordinate frame at nearly all recording levels. Since the data were acquired with the tool depth held constant for all shots, the tool orientation obtained for the far offset shots could be applied to the near offset shots. The tool orientation accuracy in the depth interval 1120-2180 m is good. For recording levels from 2200 to 3140 m (shot point 7) and from 3160 to 3920 m (shot point 5), tool orientations are less accurate due to the geometric effects of the lower direct P wave amplitudes on the horizontal components from nearer offset shot points. The horizontal components were rotated into a E-W/N-S coordinate system prior to applying standard processing methods (Table 3).

The wave fields of most shots allow us to identify five distinct reflecting events (Figure 7) that intersect the borehole at about 1400, 2000, 2300, 3050, and 3300 m (labeled B, B2, R2300, C2, and D in Figure 7). They can be related to the east dipping reflections found in the surface seismic data since they intersect the borehole at similar depths. However, no clear east dipping event is observed on the surface seismic that would correspond to R2300. The reflector at 3300 m may correspond to event D on the surface seismic. Event C on the surface seismic may be related to the reflector at 3050 m (labeled C2 in Figure 7), but the reflector appears deeper in the main hole and its reflection amplitude is much lower than that expected from the surface seismic. A less distinct event (labeled C and most clearly observed on shot 3 in Figure 7 and in the three components of shot 12 in Figure 8) intersects the borehole at about 2800 m, and it may be this event that corresponds to event C on the surface seismic. Note that the VSP97 survey started at 1120 m, below the depth expected (~1000 m) for reflector A.

Several events coming from steeply dipping interfaces can be also observed on the VSP97 data. Three of the more consistent ones are marked in Figure 7. The first (X1) intersects the borehole at ~1300 m and is observed on nearly all shots. The second (X2) intersects the borehole at ~2500 or 2600 m and has varying clarity from shot to shot. The third (X3) intersects the borehole at ~3500 m. It is difficult to accurately determine the intersection point with the borehole since these reflected events become nearly parallel to the direct wave where the reflector intersects the borehole. The steeply dipping events tend to be more prominent on shots with high-frequency content, indicating they originate from relatively thin features. The west dipping set of reflections Z is not observed on the VSP97 data

Interval velocities (Figure 3b) have been calculated for the VSP97 data by slant stacking over the 40-m intervals existing between the three recording units. First, the apparent slowness was calculated. Then it was converted to real slowness and velocity over the depth interval where the data were recorded. Since the distance between the three units on the recording tool was fixed to 20 m, no uncertainties exist regarding the depth interval between adjacent geophones. The consistency of the slowness calculation for all 15 shot points gives confidence in the interval velocity curve (Figure 3b). The average calculated V_p is 6.15 km/s. Move out analyses of the direct S wave indicate an average V_s of 3.42 km/s, giving a V_p/V_s ratio of 1.8. Median V_p and V_s of core samples are 6.18 and 3.4 km/s, respectively (Figure 4), in close agreement with the VSP velocities. Average core density is about 2.82 g/cm^3. These averaged values will be considered as valid background elastic properties when studying

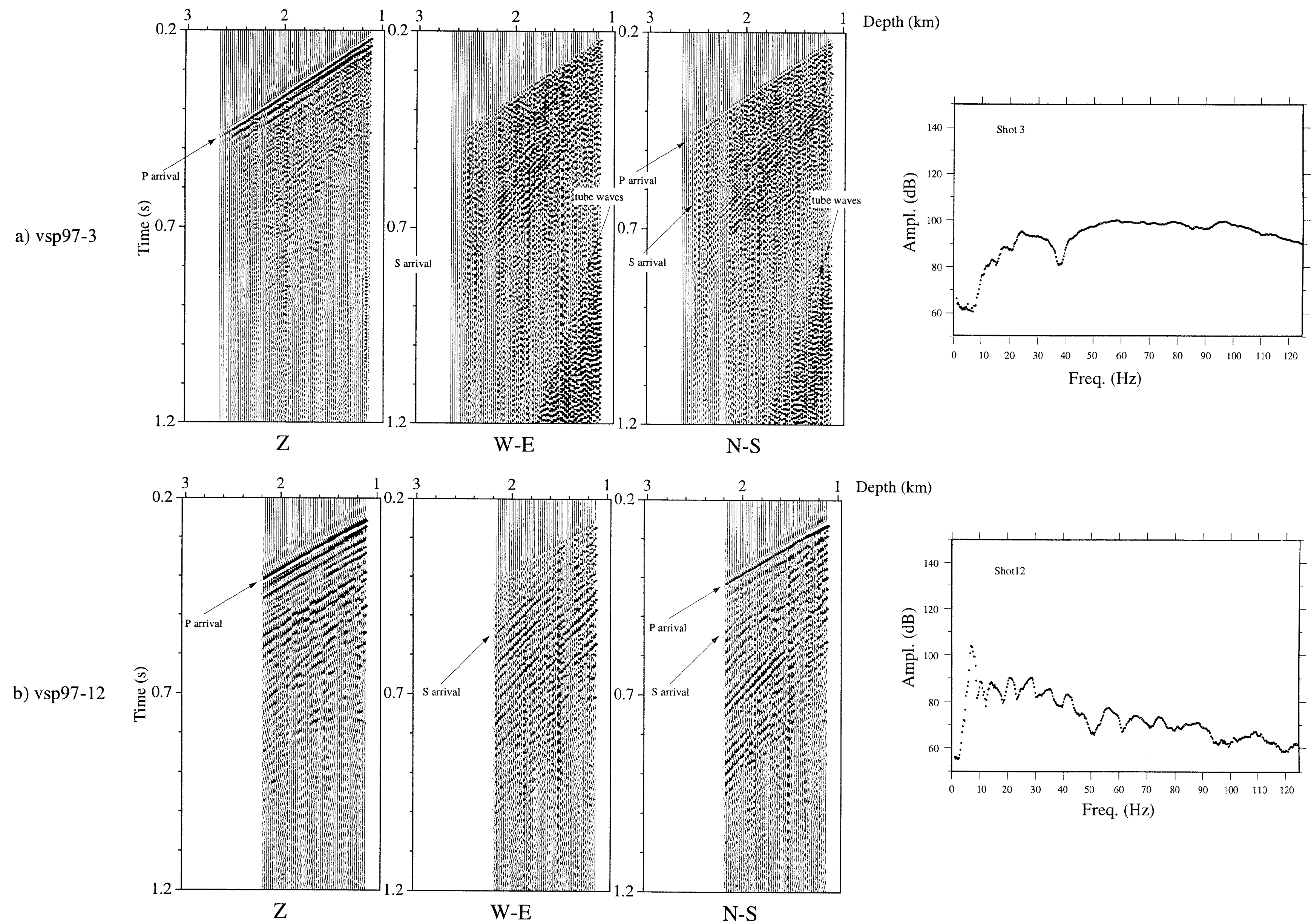

Figure 6. Data from VSP97 (a) shot point 3 and (b) shot point 12 after processing up to step 5 in Table 3. Relative amplitudes are the same for all three components. Frequency spectrum of the vertical components from both raw shots is also shown. Note that shot 12 has higher amplitudes at low frequencies than shot 3.

Table 3. Processing parameters for VSP97 data

Step	Description
1	Read SGY data
2	Scale by time
3	Pick first breaks
4	Rotate to E-W/N-S system
5	Band-pass filter: 25-40-120-180 Hz
6	Trace equalization
7	In fill-killed traces
8	Remove downgoing *P* waves, 13-point median
9	Remove downgoing *S* waves, 9-point median
10	Mute to first arrival time
11	Trace equalization
12	Remove >4500 m/s waves, 13-point median, SP1-7
	Remove ∞ m/s waves, 13-point median, SP8-15
13	F-X Decon, 30-100 Hz

deviations along the borehole which may cause seismic reflections.

8. VSP94 Three-Component Processing and Interpretation

The VSP94 data were acquired over a depth range of 520 to 3940 m, thus allowing shallower events to be observed. In previous work [*Juhlin et al.*, 1997] only the results from the vertical component data were presented. They showed reflections intersecting the borehole at depths close to those found for the VSP97 data. We interpret depths of intersection slightly differently here because there are more shots on which to base our interpretation (15 shots in VSP97 versus 2 shots in VSP94). Strong variation in the data quality and seismic response appear to be typical for this site.

Figure 9 shows the three-component VSP94 data after rotation to a E-W/N-S orthogonal system and subsequent processing to remove downgoing *P* and *S* waves. The reprocessed data show a very steep event on the E-W component which intersects the borehole at ~2500 m (X2? in E-W of Figure 9). It probably corresponds to X2 on the VSP97 sections (Figure 7). Its low amplitude on the N-S component and its move out suggest that it originates from a ~N-S striking interface that dips steeply to the east. A weaker event arriving at near infinite apparent velocity in the vertical component (X2? in Z component of Figure 9) appears to intersect the borehole at about the same depth and could correspond to a *P* to *S* converted wave from the same interface. Another high-amplitude event on the VSP94 data observed at ~0.7 s on the vertical component has an apparent velocity close to infinity (X3? in Z component of Figure 9). An *S* wave reflecting off a steeply east dipping interface west of the borehole will have a high amplitude on the vertical component and arrive at near infinite apparent velocity for the VSP94 SP2 geometry. X3 is projected to intersect the borehole at ~3500 m, and thus this event may correspond to a *P* to *S* converted wave reflection from the X3 reflector in Figure 7. This event and other weaker ones below with similar high apparent velocity probably correspond to the steep events observed on the VSP97 data (Figure 7). The *P* wave reflection corresponding to the probable X3 event is not clearly observed in the data although some signs of it are present in the E-W component.

A dipping reflection probably originating from reflector A (Plate2 and Figure 5) also appears as a clear event on the vertical component seismogram in the VSP94 data (Figure 9). Events with similar move out velocity are also present below this event and probably originate from *P* to *S* converted waves of the east dipping set of reflectors (B-D in Figure 7).

9. VSP Modeling

9.1. Modeling Method

For modeling purposes we define two different types of reflectors. The first is a "mafic" reflector that consists of higher-velocity and higher-density material when compared to the host rock. It has a lithological origin (e.g., dolerite sills of *Juhlin et al.* [1990]). Several steeply dipping mafic dikes intersect the borehole, especially in the depth range 3000-4000 m [*Bashta et al.*, 1990]. These generally dip 60-70° to the west and are ~5 m

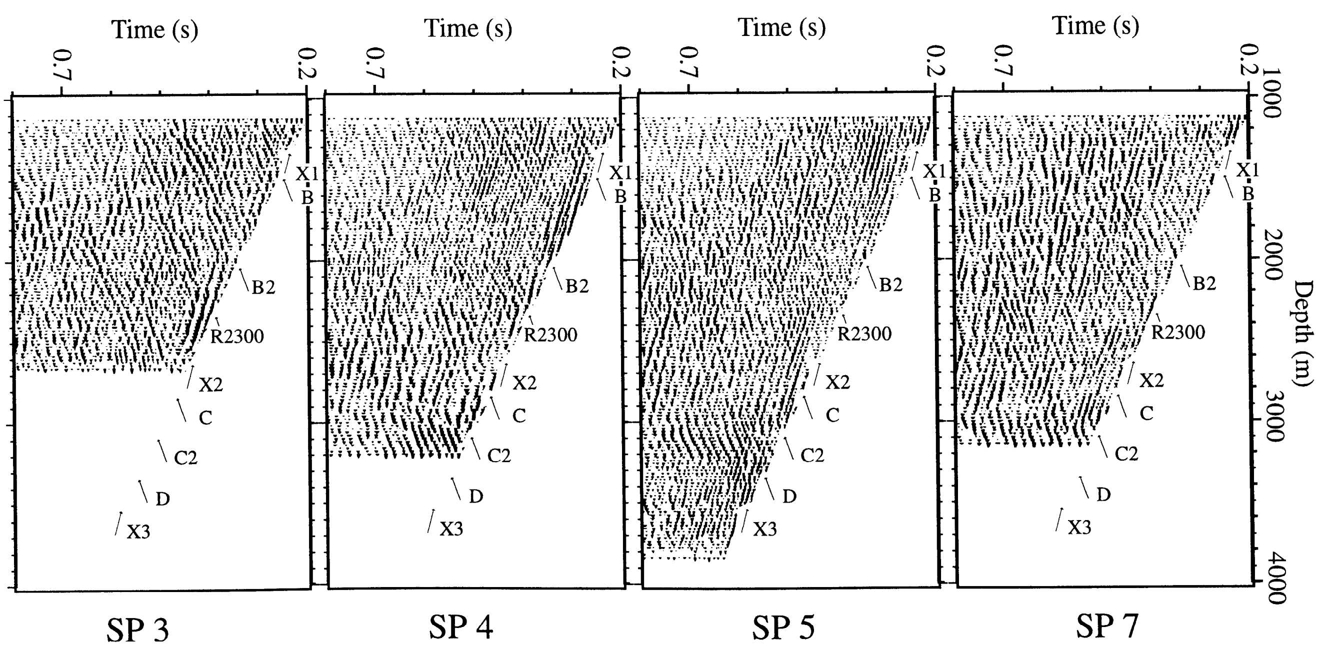

Figure 7. Processed vertical component data from shot points 3, 4, 5, and 7.

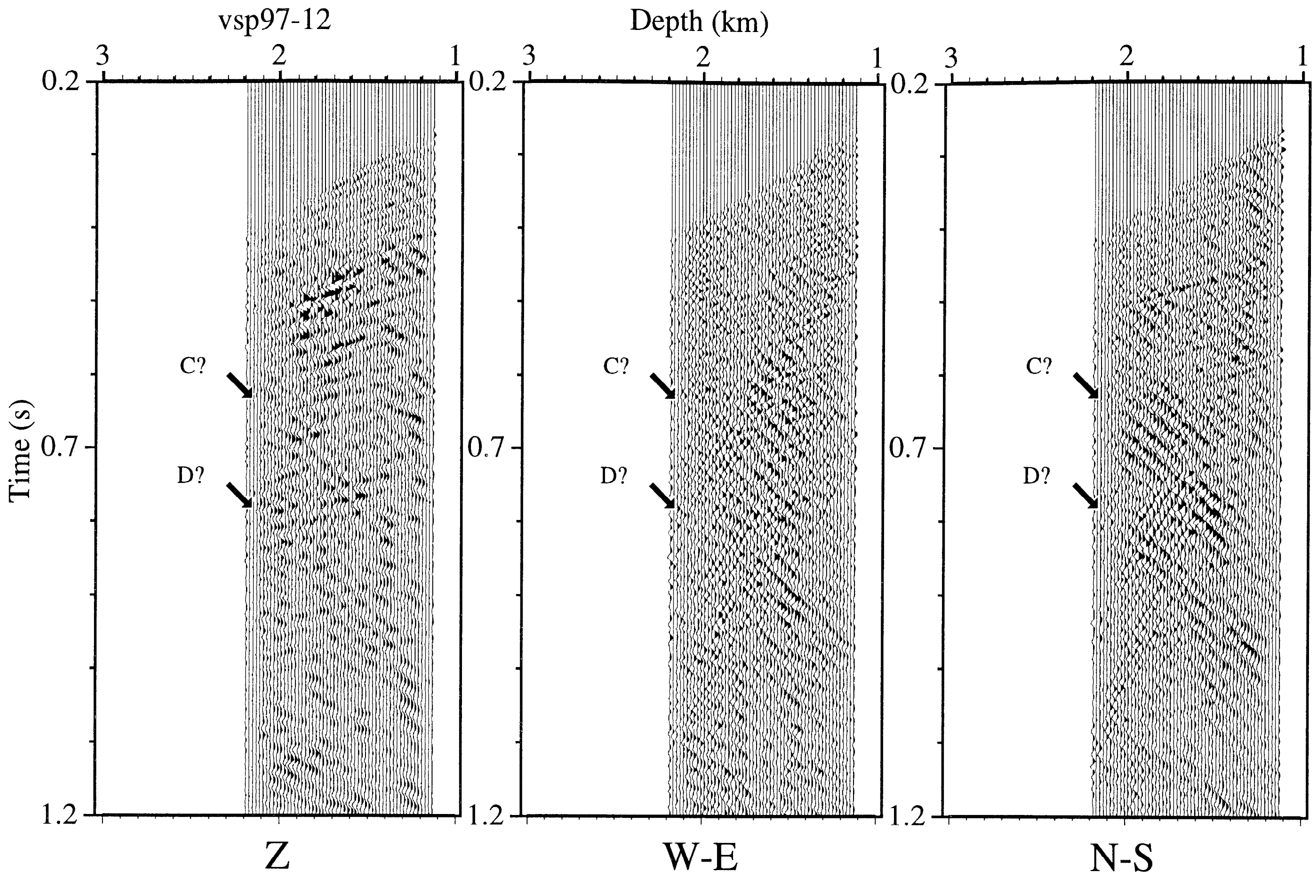

Figure 8. Data from VSP97 shot point 12 after processing up to step 14 in Table 3. The events C? and D? are picked on the basis of its amplitude and coherency in the three components.

thick and constitute a possible source of the reflectivity arriving parallel to the interpreted X set of reflections. The second type is a "fracture zone" whose material has lower velocities and densities than the host rock. The fracture zone name implies increased primary or secondary porosity. In a volcanic setting such as the Tagil Arc, lava flows and pyroclastic units intercalated with sediments may have a similar porosity to tectonically induced fracture zones. From a seismic viewpoint it is not possible to differentiate between the two origins of the increased porosity, although the tectonic fabric associated with faults would be more anisotropic and tend to be more reflective [*Ganchin et al.*, 1998].

The modeling presented here is carried out in five steps: (1) the travel times to the top of the reflector are calculated from the geometry of the shot point, receiver point, the strike and dip of the reflector, and its intersection point with the borehole (Table 4), (2) the angle of incidence at the reflector is determined and the appropriate reflection coefficients for P and S wave reflections are assigned using published equations [*Aki and Richards*, 1980], (3) the interference effect of a thin layer is taken into account [*Juhlin and Young*, 1993], (4) the angles of arrival at the receiver point are determined and the corresponding amplitude and arrival time of the event for the three components are assigned giving a spikogram, and (5) the spikograms are convolved with a source wavelet. We assume the velocity above the reflector to be constant, a reasonable assumption for the SG4 case, and the reflector to be a simple interface or a thin layer imbedded in a homogeneous medium. Since the elastic contrasts are relatively small, other factors affecting the reflection waveform such as transmission losses and multiples can be ignored within the thin layer. Even though the elastic contrasts are rather small, the effect of angle of incidence on the reflection coefficient is significant over the range 0-60° (Figure 10), and this is accounted for in the modeling. However, phase changes in the reflected waveform of postcritical reflections are not included. Comparison of the modeling method presented here with elastic finite difference solutions [*Frenje and Juhlin*, 1998; *Levander*, 1988] to thin layer models using the elastic properties given in Table 5 show good agreement up to the critical angle. Beyond it, reflection amplitudes are higher from the finite difference modeling.

In order to examine the difference in response between a mafic reflector and a fracture zone reflector we must assign elastic properties to the surrounding host rock and the reflectors. For the volcano-sedimentary host rock we assume it to have the average elastic properties measured on core. It is more difficult to assign values to the reflectors, especially the fracture zones, since in situ V_s are not available. Assumptions based on the available data and results from other studies [e.g., *Rudnick and Fountain*, 1995; *Takeuchi and Simmons*, 1973; *Juhlin et al.*, 1991; *Pedersen et al.*, 1992; *Ganchin et al.*, 1998; *Koslovsky*, 1987; *Harjes et al.*, 1997; *Digranes et al.*, 1996] are those given in Table 5. Since minor changes in the V_p/V_s ratio will only result in minor changes in the reflection coefficient curves (Figure 10)

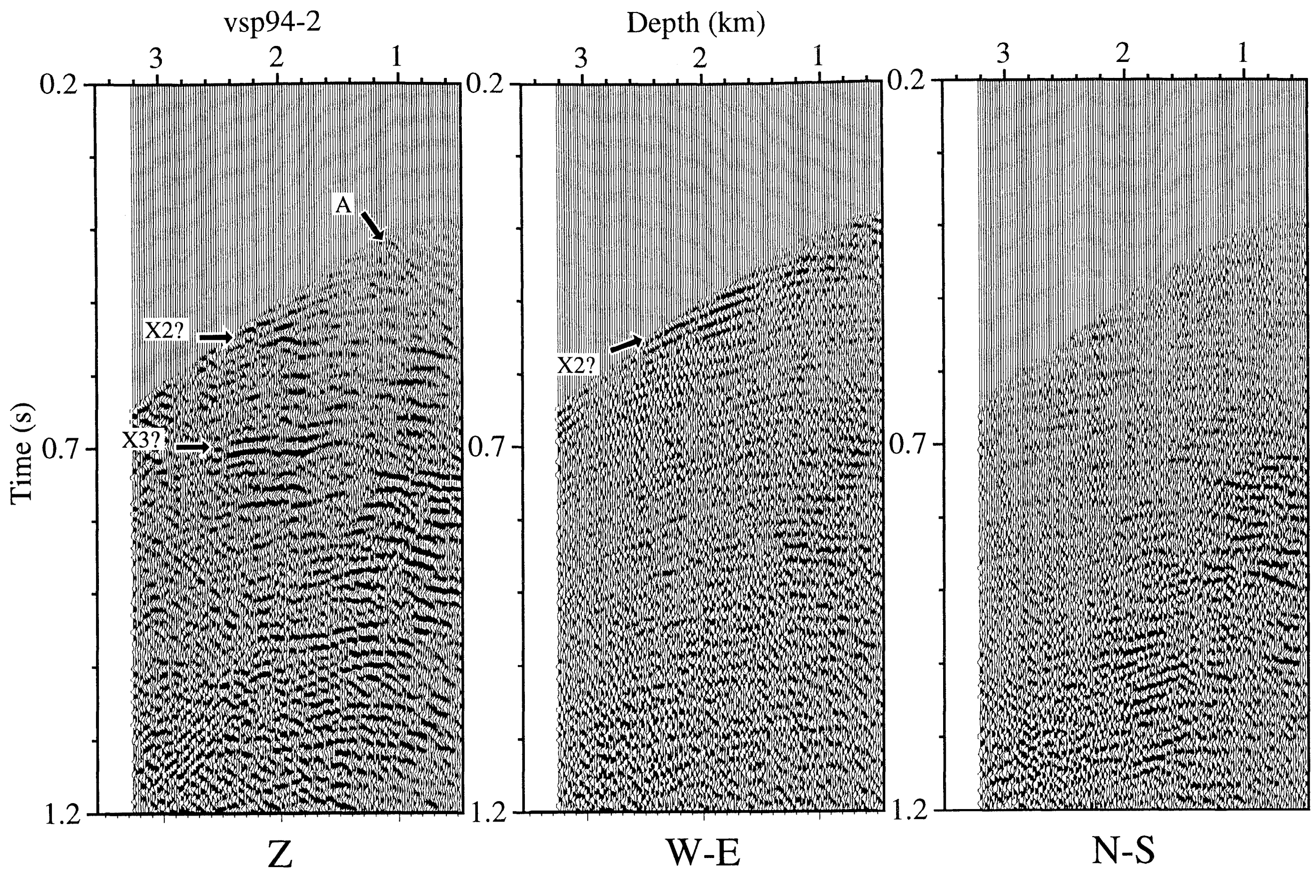

Figure 9. Three-component data from the far offset VSP94 shot point after removal of the downgoing *P* and *S* waves. Relative amplitudes are the same for all three components. Note that this shot point is located ~2 km east of the borehole (Plate 1). This implies that different subsurface geometries are illuminated and that events originating from the same interfaces as on the VSP97 data will have different travel time curves.

the results from the seismic modeling should be generally valid for comparing the response between the mafic and fracture zone models.

9.2. Modeling Results

Comparison of the Z component of the synthetic seismograms from both the mafic model (Figure 11a) and the fracture zone model with the VSP94 and 97 data (Figure 11b) shows that for the east dipping events (B, B2, R2300, C, C2, and D) the latter have more of the characteristics observed in the real data (Figure 7). For the mafic model the reflected *P* wave energy from the east dipping set of events is on the same order as the reflected *P* to *S* converted wave energy. For the fracture zone model, mainly reflected *P* to *S* converted wave energy is observed. In both models, very little *P* wave energy is expected to be reflected close to the points where the reflectors intersect the borehole. The persistence of the *P* to *S* converted wave reflections and the lack of clear *P* wave reflected arrivals in Figure 11b suggests that fracture zones are a more likely source of the east dipping set of reflections. Varying the thickness of the reflectors gives similar results as those presented in Figure 11.

Table 4. Depth of the Intersection Point in the Borehole and Strike, Dip, and Thickness of the Modeled Reflectors

Event	Depth, m	Strike, deg	Dip, deg	Thickness, m
B	1400	N355	40	20
B2	2000	N355	45	20
R2300	2300	N355	45	20
C	2800	N355	45	20
C2	3050	N355	45	20
D	3300	N355	45	20
X1	1300	N355	75	20
X2	2600	N355	75	20
X3	3500	N355	75	20

Modeling of reflectors that intersect the borehole below the survey limit of shots 8-15 suggest that the prominent reflection at about 0.7 s on the N-S component from shot 12 (C? in Figure 8) corresponds to a *P* to *S* converted reflection off a ~N-S striking reflector, dipping at 35°E and intersecting the borehole at 2800 m. The *P* to *S* converted wave energy, however, should be strongest on the E-W component, indicating that this event may not originate from reflector C. The almost equally prominent event arriving about 150 ms after event C (marked as D?) could represent a *P* to *S* converted wave reflection off reflector D, although it might as well represent the strong multiple or near-surface *P* wave reflection arriving about ~130 ms after the direct downgoing *P* wave in Figure 6b.

The steep dips suggested for reflectors X1 to X3 imply angles of incidence which are beyond critical in the deeper sections of

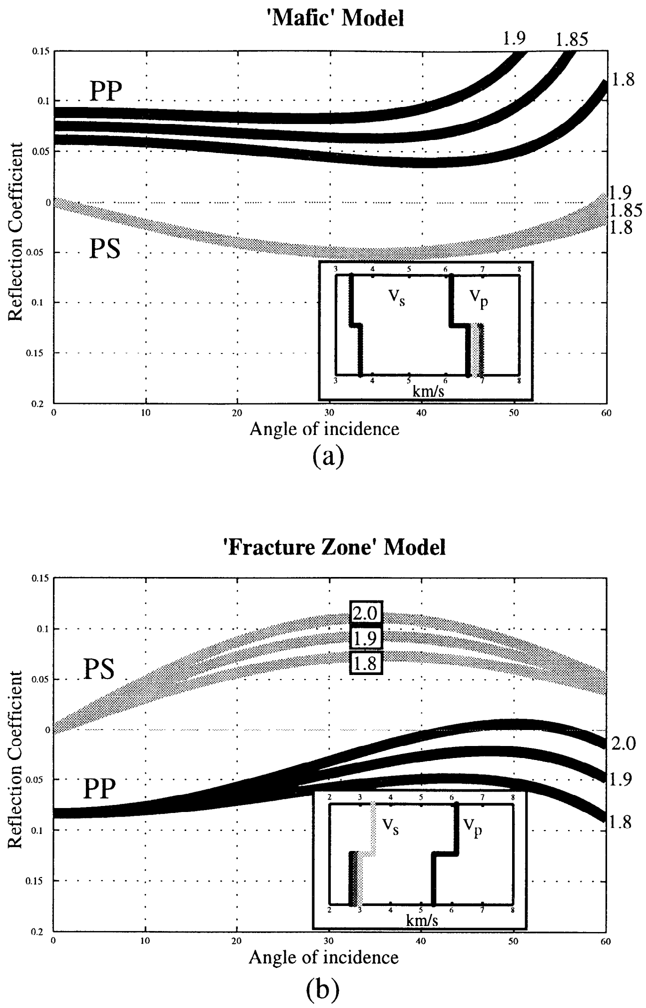

Figure 10. Reflection coefficient versus angle of incidence for two possible seismic reflectors: (a) a mafic sill and (b) a fluid-filled fracture zone. In both cases the overlying host rock has elastic properties similar to those observed for the volcano-sedimentary rocks in the SG4 borehole. Numbers on curves refer to V_p/V_s ratio.

the synthetic seismograms (arrivals below critical angle (CA) in Figure 11a) for the mafic model. The amplitude of the reflected *P* wave below these depths is artificially low and the phase is incorrect, but the travel times are correct. More advanced 2-D finite difference modeling shows that the reflected *P* wave from these steep interfaces maintains a higher amplitude from the CA point until the event intersects the borehole. Noting that the X1 to X3 reflected amplitudes below CA in Figure 11a are higher than shown, then the fracture zone model again matches the observed data better than the mafic model for reflections coming from steep interfaces, i.e., *P* wave reflected energy dominates the mafic model, while *P* to *S* converted wave energy becomes more important on the fracture zone model. This suggests that it is also more likely that the steep events originate from fracture zones. Further modeling suggests that the high amplitude event at 0.7 s observed in VSP94 (X3? in Figure 9) is a *P* to *S* converted wave that has been reflected off the X3 reflector intersecting the borehole at ~3500 m. Additionally, the steeply dipping event X2 in the E-W component in Figure 9 can be modeled as a *P* wave reflection from an interface striking approximately N-S and dipping at ~75° to the east. A weaker event arriving at near infinite apparent velocity on the vertical component and appearing to intersect the borehole at ~2500 m (X2? in the Z component of Figure 9) could correspond to a *P* to *S* converted wave reflection from this interface. Steeply dipping (70-85°) reflectors have also been observed on VSP data from the Canadian Shield when testing seismic methods for mineral exploration [*Eaton et al.*, 1996].

Reflection A in the vertical component of the VSP94 (Figure 9) and parallel ones below it can also be modeled as *P* to *S* converted waves generated on the east dipping set of reflectivity. The fact that much of the observed reflectivity on the vertical component on both the VSP94 and the VSP97 data corresponds to reflected *P* to *S* converted waves implies that the migration algorithm applied in previous work (Kirchhoff *P* wave depth migration, see Figure 9 of *Juhlin et al.* [1997]) was inappropriate. Use of a migration algorithm that takes into account *P* to *S* wave conversions is necessary and would probably give a better match between the surface seismic and VSP94 migrated sections.

10. Discussion

The ESRU95 E-W CDP line lies ~600 m north of the SG4 borehole along the strike of the structures. Reflectivity on this line is interpreted to represent geological features found within the borehole, although it is not clear that a reflection can be attributed to any one geological feature.

Reflectors C and D intercept the borehole in the LVDR zones at ~2900 and 3400-3500 m. The density contrast in those intervals never exceeds 0.12 g/cm^3 (i.e., <5%). The changes in V_p, however, reach 1.9 and 2.1 km/s, respectively, (i.e., ~33%). Therefore, at these depths, V_p has a greater influence on the seismic impedance (i.e., reflectivity) than the density (Figure 3a). Assuming that no event disrupts the structure of the Tagil Arc between the ESRU95 E-W line and the SG4 borehole, we argue that it is mostly the low velocity associated with the LVDR zones located at ~2900 and ~3400 m in the borehole that gives rise to reflectors C and D. The predominance of *P* to *S* conversions in the VSP data at those depths (Figure 7) suggests that the fracture zone model fits the data better, thus supporting this interpretation.

The source of reflectors A and B, interpreted from surface seismics and VSP data to intercept the borehole at ~1000 m and ~1500 m, respectively, is more ambiguous since they do not coincide with wide LVDR zones. Instead, narrow diorite and dolerite intrusions associated with low V_p zones have been described at those depths in the borehole (Figure 3). Reflector A does not appear to correspond to density variations related to the intrusions since values range from 2.8 to 2.87 g/cm^3 in the interval around 1000 m. Variations in V_p are, however, higher (V_p=5.15-6.1 km/s). Similarly, reflection B might be caused by a narrow high density zone at ~1460-1490 m (2.9-2.92 g/cm^3) that implies a density contrast less important than that of a local low V_p zone at ~1490 m (V_p =3.5 km/s on the wire line log data). Considering that (1) V_p variations at this depth are around one order of magnitude higher than density variations and (2) the *P* to

Table 5. Elastic Properties of the Rocks Assumed in the Seismic Modeling

Rock Type	V_p, m/s	V_s, m/s	Density, g/cm^3	V_p/V_s
Volcano-sedimentary	6150	3420	2.88	1.8
Fracture zone	5400	2700	2.7	2.0
Mafic	6900	3630	3.0	1.9

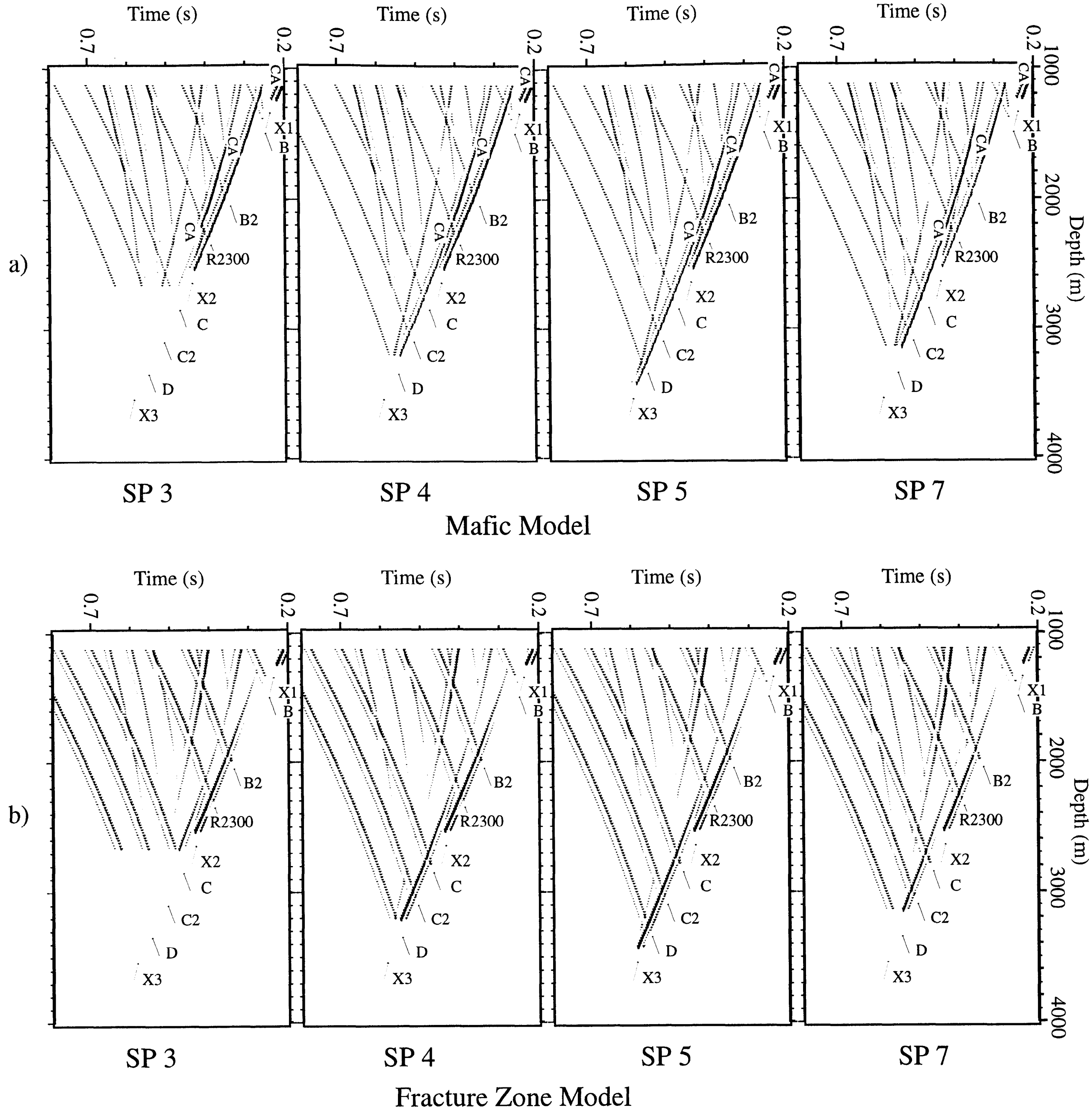

Figure 11. Modeling of the marked events in shots 3, 4, 5, and 7 in Figure 7 using (a) a mafic reflector model and (b) a fracture zone reflector model. All models correspond to the vertical (Z) component. Elastic properties used are given in Table 5, and the reflector geometries used are given in Table 4. CA; critical angle for the modeling geometry of high impedance reflector.

S conversions present in the fracture zone model for reflectors A and B fit better the real VSP data, we suggest that both reflections are primarily due to hydrothermally altered (chlorite, epidote) low V_p zones. These low V_p zones are associated with the diorite and dolerite intrusions and their corresponding density contrasts may influence the reflectivity.

Reflector E is interpreted to intercept the borehole in a wide zone between ~4000-5400 m. It can be tentatively correlated with a zone of high reflectivity observed below the bottom of the VSP94 and VSP97 experiments but not included in the modeling (see *Juhlin et al.* [1997] for an example on VSP94). At the surface, it coincides with the East Arbat Fault [*Sokolov*, 1991], which is associated with a lithological contrast marked by a gravity and magnetic anomaly. Density variations at 4000-5400 m depth are much less than V_p variations (2.74-2.94 g/cm^3 versus 5.55-6.25 km/s, respectively). Thus reflector E should correspond to the V_p variations associated with the East Arbat Fault Zone, although changes in lithology, and thus density across this zone may play a role.

Reflectors F and G do not intersect the borehole. Their reflectivity may be associated with the Arbat Massif and the West Arbat Fault, respectively, but the relative contributions of

V_p contrast or contrasting densities/lithologies to the reflectivity are not known.

LVDR zones appear to be one of the causes of reflectivity in the ESRU profiles, although not all of them are reflective. For example, no clear reflectivity can be attributed to the LVDR zone at ~3800 m in the pilot hole. The interval velocities derived from the VSP97 data (shot 5) recorded in the main hole (Figure 3b) do not mark a pronounced low V_p zone at this depth, although they do decrease. The LVDR zone at ~3800 m might be related to the clear east dipping reflectivity that exists between 4000 and 5400 m. However, we suggest that it probably represents a zone wituout lateral continuity.

The highest densities in the borehole (2.85-2.96 g/cm^3) are found at 2500 m where V_p reaches 6.28-6.66 km/s but dropping to 3.9 km/s at 2520 m. These density and velocity values suggest the presence of a diorite dike, but no dike is noted in the lithology description at this level. The ESRU95 E-W surface seismic section does not show marked reflectivity at this depth yet the zone is thick enough (~60 m) to be resolved by it. The VSP data show that X2 (Figures 7 and 9), which intercepts the borehole at ~2500 m, represents a steeply east dipping interface that may be too steep to be imaged by surface seismic data or may lack lateral continuity. *P* to *S* conversions suggest that it is the low V_p interval at 2520 m which gives the reflectivity in the VSP data. The small variation of density compared to the high contrast in V_p at this depth supports this interpretation.

The VSP97 experiment was shot with the goal of further constraining the location away from the borehole of reflector C, not a prominent one in the VSP94 data [*Juhlin et al.*, 1997]. At ~2900 m, the expected depth of the C reflector, the main hole lies ~100 m south of the pilot hole (Figure 2). A highly fractured zone observed in the pilot hole from about 2900 to 3050 m is not observed in the main hole [*Juhlin et al.*, 1997]. Borehole to borehole correlations based on cuttings and cores indicate depth differences of similar lithologies of ~100 m at these depths. Considering the trajectory of the two holes at depth, a ~N355° trending, 35°E dipping LVDR zone found in the pilot hole at 2900 m depth would be expected (if it were continuous) in the main hole farther to the south at a slightly greater depth (~2940-3000 m). The projection of this LVDR zone from the pilot hole to the main hole indicates that it may be reflector C2 at 3050 m, observed on many of the VSP97 shots (Figure 7), that correlates with reflector C in the surface seismic data. Alternatively, reflector C at 2800 m in shots 11-15 (Figure 8) and 3 (Figure 6) from the VSP97 has more of the characteristics observed in the surface seismic data (e.g., high amplitude) and can be correlated with the LVDR zone at ~2900 m. C and C2 may represent the upper and lower parts of reflector C in the surface seismic data that are imaged separately due to the higher resolution of the VSP data. However, processing of the VSP97 data using the same frequency band as the surface seismic data does not enhance reflector C. In addition, the frequency content of the VSP94 data was lower than that of the VSP97 data and reflector C was even less clear.

We suggest that the irregular reflectivity associated to reflector C may be related to changes of its physical properties along strike. Accordingly, the ESRU95 N-S line (Plate 2) shows that reflector C and D become weak where the SG4 borehole projects onto the line, indicating lateral changes in the reflectivity. In shots 11-15 the reflection points for such an event fall close to the plane of the E-W surface seismic line (Plate 1) where event C has high amplitude. The implied stronger impedance contrast at this location may be due to (1) increased porosity at this location, implying more fluids and/or more anisotropy, (2) the surrounding rock is more homogeneous, and (3) the high porosity zone is here bounded by highly mafic rock which increases the composite reflection coefficient.

11. Conclusions

Contrary to other Paleozoic arcs (Magnitogorsk [*Brown et al.*, 1998]) and modern arcs (Banda [*Snyder et al.*, 1996]) the Tagil Arc appears to be highly reflective. The SG4 borehole, located in the western part of the Tagil Arc, provides an excellent opportunity to accurately locate the reflectors and to address the source of their reflectivity. The main reflectors interpreted from surface seismics strike ~N355° and dip ~35°-55° to the east. They intercept the borehole at ~1000, 1500, 2800-2900, 3400-3500 m, and between ~4000 and 5400 m and coincide with the low-velocity/low-density/low-resistivity (LVDR) zones. These zones are interpreted to be fluid-filled high-porosity intervals that are often associated with lithological changes. Many of these intervals have been considered as tectonic contacts [*Bashta et al.*, 1996]. This interpretation is supported by recent reports on the tabular morphology of pyrite crystals found within these zones [*Dokuchaev et al.*, 2000]. Reflectivity in fault zones is thought to be caused by a complex pattern of compositional and strain induced ductile anisotropic effects [*Christensen and Szymansky*, 1988]. However, *Ganchin et al.* [1998] argue that in the Kola borehole anisotropy due to preferred mineral orientation should not lower velocities more than 5% and suggest that fluid-filled voids is the most important mechanism for generating subhorizontal reflections. This is in accordance with our studies in the SG4 borehole where high porosities found in hidrothermally altered core samples cause a decrease in V_p of up to ~33%, thereby enhancing the reflectivity.

In general, clear *P* to *S* converted wave reflections are observed on the VSP data where vertical incidence reflections are predicted to cut the borehole. Modeling also suggests that fracture zones (implying low-velocity porous zones), rather than mafic dikes (implying denser, higher-velocity intervals), are the most likely explanation for the source of this east dipping reflectivity. In addition, VSP data show reflections originating from structures dipping at 70-75° to the east that also appear to be related to fracture zones. These reflections are not observed on the surface seismic data.

The most prominent event on the E-W surface seismic line, ~600 m north of the SG4 borehole, has a corresponding high-amplitude signature in the northernmost VSP shots where strong *P* to *S* converted waves correlate with this event. Since the reflection points for those shots lie approximately below the E-W surface seismic line, we argue that strong changes in the physical properties of the reflector along strike cause its varying reflectivity.

We interpret the LVDR zones related to high reflectivity on surface and VSP seismic data as areas of increased primary or secondary porosity that are probably filled with fluids. Tectonic criteria and the geometry of the reflectors indicate that they might be imbricated fractures often parallel to lithological boundaries. These zones could have been reactivated by sinistral strike slip that may have imparted a fabric to the rocks that further enhanced reflectivity [*Ayarza et al.*, 2000]. Lateral changes of facies and unconformities, common in volcanic environments, might, also, explain the pattern that the reflectivity exhibits in this area.

Acknowledgments. P. Ayarza is funded by the EU TMR program by the UE-TMR project URO (ERBFMRXCT960009). The VSP97 experiments were financed by the same project and were coordinated in Russia by the Bazhenov Geophysical Expedition and NEDRA. C. Juhlin is funded by the Swedish Natural Sciences Research Council (NFR). Geoffrey Kimbell and Conxi Ayala publish with the permission of the director of the BGS (NERC). The Swedish Nuclear Waste Management Co. (SKB) financed a visit by L. Pevzner and R. Pevzner to Uppsala University in September 1998. Magnus Friberg aided us in preparing the magnetic data. We thank D. Snyder, D. Smythe, and H.P Harjes for their helpful comments. This is an EUROPROBE publication.

References

Aki, K., and P.G. Richards, *Quantitative Seismology*, 1, 557 pp., W.H. Freeman, New York, 1980.

Ayarza, P., D. Brown, J. Alvarez-Marrón, and C. Juhlin, Contrasting tectonic history of the arc-continent suture in the Southern and Middle Urals: implications for the evolution of the orogen, *J. Geol. Soc.*, in press, 2000.

Barton, P. J., The relationship between seismic velocity and density in the continental crust-A useful constraint?, *Geophys. J. R. astron. Soc.*, *87*, 195-208, 1986.

Bashta, E.G., V.N. Kushkov, L.N. Shaktornaya, A.N. Glushkov, and V.A. Sergeev, First results from the drilling and investigations of the superdeep borehole (SG4) (in Russian), *Min. Geol. SSSR*, *1*, 19-30, 1990.

Bashta, E.G., V.A., Gorbunov, A.Y., Dokuchaev, V.V. Kenig, A.A. Nosova, and V.I. Segalovich, Main objectives and results of the investigations at the Urals Superdeep Well (in Russian), *Explor. Preserv. Miner. Resour.*, *7*, 6-9, 1996.

Bliznetsov, M., and C. Juhlin, Analyses of wavefields by the common excitation array (CEA) method, *J. Appl. Geophys.*, *32*, 245-256, 1994.

Brown, D., C. Juhlin, J. Alvarez-Marrón, A. Pérez-Estaún, and A. Oslianski, Crustal-scale structure and evolution of an arc-continent collision zone in the southern Urals, Russia, *Tectonics*, *17*,158-171, 1998.

Christensen, N.I., and D.L. Szymansky, Origin of reflections in the Brevard fault zone, *J. Geophys. Res.*, *93*, 1087-1102, 1988.

Digranes, P., Y. Kristoffersen, and N. Karajev, An analysis of shear waves observed in VSP data from the superdeep well at Kola, Russia, *Geophys. J. Int.*, *126*, 545-554, 1996.

Dokuchaev, A. Y., G.V. Tarkhanov, A.G. Gurbanov, A.F. Morozov, A.A. Nosova, K.G. Bashta, D.I. Krinov, and A.I. Tsepin, Metamorphic hydrothermal golden mineralization in the Imennovian Suite of the Tagil trough (by materials of drilling the Urals Superdeep Well), *Explor. Preserv. Miner. Resour.*, in press, 2000.

Eaton, D., S. Guest, B. Milkereit, W. Bleeker, D. Crick, D. Schmitt, and M. Salisbury, Seismic imaging of massive sulfide deposits, part III, Borehole seismic imaging of near-vertical structures, *Econ. Geol.*, *91*, 835-840, 1996.

Echtler, H.P. et al., Preserved collisional crustal structure of the Southern Urals revealed by vibroseis profiling, *Science*, *275*, 224-225, 1996.

Frenje, L., and C. Juhlin, Scattering of seismic waves simulated by finite difference modeling in random media: Application to the Gravberg-1 well, Sweden, *Tectonophysics*, *293*, 61-68, 1998.

Friberg, M., and G.A. Petrov, Structure of the Middle Urals, east of the main Uralian fault, *Geol. J.*, *33*, 37-48, 1998.

Ganchin, Y.V., S.B. Smithson, I.B. Morozov, D.K. Smythe, V.Z. Garipov, and N.A. Karaev, Seismic studies at the Kola Superdeep Borehole, Russia, *Tectonophysics*, *288*, 1-16, 1998.

Green, A.G., and J.A. Mair, Subhorizontal fractures in a granitic pluton: Their detection and implications for radioactive waste disposal, *Geophysics*, *48*, 1428-1449, 1983.

Harjes, H.P. et al., Origin and nature of crustal reflections: Results from integrated seismic measurements at the KTB superdeep drill site, *J. Geophys. Res.*, *102*, 18,267-18,288, 1997.

Holliger, K., A.G. Green, and C. Juhlin, Stochastic analysis of sonic logs from the upper crystalline crust: Methodology, *Tectonophysics*, *264*, 341-356, 1996.

Juhlin, C., Interpretation of the reflections in the Siljan Ring based on results from the Gravberg-1 borehole, *Tectonophysics*, *173*, 345-360, 1990.

Juhlin, C., and R. Young, Implications of thin layers for amplitude variation with offset (AVO) studies, *Geophysics*, *58*, 1200-1204, 1993.

Juhlin, C., A.A. AlDahan, J. Castano, B. Collini, T. Gorody, and H. Sandstedt, Scientific summary report of the Deep Gas Drilling Project in the Siljan Ring impact structure, Vattenfall, Stockholm, 1991.

Juhlin, C., S. Kashubin, J.H. Knapp, V. Makovsky, and T. Ryberg, Project conducts seismic reflection profiling in the Ural Mountains, *Eos. Trans. AGU*, *76*, 193-199, 1995.

Juhlin, C., M. Bliznetsov, L. Pevzner, T. Hismatulin, A. Rybalka, and A. Glushkov, Seismic imaging of reflectors in the SG4 borehole, Middle Urals, Russia, *Tectonophysics*, *276*, 1-18, 1997.

Juhlin, C., M. Friberg, H. Echtler, T. Hismatulin, A. Rybalka, A. Green, and J. Ansorge, Crustal structure of the Middle Urals: Results from the Europrobe Seismic Reflection Profiling in the Urals (ESRU) experiments, *Tectonics*, *17*, 710-725, 1998.

Karetin, Y.S., A structural position and facial-formational belonging of volcanogenic deposits in the Ural superdeep well (SG-4), The Urals superdeep well (interval of 0-4008) (in Russian), *Geology, Geophysics, Technology*, pp. 158-165, GNPP Nedra, Yaroslavl, 1992.

Knapp, J.H., C.C. Diaconescu, M.A. Bader, V.B. Sokolov, S.N. Kashubin, and A. V. Rybalka, Seismic reflection fabrics of continental collision and post-orogenic extension in the Middle Urals, central Russia, *Tectonophysics*, *288*, 115-126, 1998.

Koslovsky, Y.A., *The Superdeep Well of the Kola Peninsula*, Springer-Verlag, New York, 1987.

Levander, A.R., Fourth-order finite-difference *P-SV* seismograms, *Geophysics*, *53*, 1425-1436, 1988.

Ludwig, J.W., J.E. Nafe, and C.L. Drake, *Seismic Refraction in the Sea*, vol. 4, edited by A.E. Maxwell, John Wiley, New York, 1970.

Lüschen, E., K. Bram, W. Söllner, and S. Sobolev, Nature of the reflections and velocities from VSP experiments and borehole measurements at the KTB deep drilling site in southeast Germany, *Tectonophysics*, *264*, 309-326, 1996.

Miao, X., W.M. Moon, B. Milkereit, and C.J. Mwenifumbo, Three component vertical seismic profiling (VSP) experiment in the Sudbury Basin, *Geophys. Res. Lett.*, *21*, 939-942, 1994.

Nafe, J.E., and C.L. Drake, Variation with depth in shallow and deep water marine sediments of porosity, density and the velocities of compressional and shear waves, *Geophysics*, *22*, 523-552, 1957.

Pavlenkova, N.I., The Kola Superdeep Drillhole and the nature of seismic boundaries, *Terra Nova*, *4*, 117-123, 1992.

Pedersen, L.B., T.M. Rasmussen, and C. Juhlin, Electric resistivity in the Gravberg-1 deep well, Sweden, *J. Geophys. Res.*, *97*, 9171-9182, 1992.

Puchkov, V.N., Structure and geodynamics of the Uralian Orogen, in Orogeny through time, edited by J.P. Burg and M. Ford, *Geol. Soc. Spec. Publ*. *121*, 201-236, 1997.

Rudnick, R.L., and D.M. Fountain, Nature and composition of the continental crust: A lower crustal perspective, *Rev. Geophys.*, *33*, 267-309, 1995.

Snyder, D.B., H. Prasetyo, D,J, Blundell, C.J. Pigram, A.J. Barber, A. Richardson, and S. Tjokosaproetro, A dual doubly vergent orogen in the Banda Arc continent-arc collision zone as observed on deep seismic reflection profile, *Tectonics*, *15*, 34-53, 1996.

Sokolov, V., The deep structure of the Central Urals, in Europrobe Symposium, edited by D.G. Gee and M. Beckholmen, p. 173, Polish Acad. Sci., Jablona, Poland, 1991.

Steer, D.N., J.H. Knapp, L.D. Brown, A.V. Rybalka, and V.B. Sokolov, Crustal structure of the Middle Urals based on reprocessing of Russian seismic reflection data, *Geophys. J, Int.*, *123*, 673-682, 1995.

Takeuchi, S., and G. Simmons, Elasticity of water-saturated rocks as a function of temperature and pressure, *J. Geophys. Res.*, *78*, 3310-3320, 1973.

Vernik, L., S. Hickman, D. Lockner, and M. Rusanov, Ultrasonic velocities in core from the Kola superdeep well and the nature of subhorizontal seismic reflections, *J. Geophys. Res.*, *99*, 24,209-24,219, 1994.

Zalewski, E., D. Eaton, B. Milkereit, B. Roberts, M. Salisbury, and L. Petrie, Seismic reflections from subvertical dikes in Archean terrane, *Geology*, *25*, 707-710, 1997.

Zhivkovich, A. Y., and P.A. Chekhovich, Structure of the central part of the Ufa amphitheater, Central Urals, *Geotectonics*, *20*, 129-141, 1986.

C. Ayala and G. Kimbell, Regional Geophysics Group, British Geological Survey, Keyworth, Nottingham, England, U.K.

P. Ayarza, Departamento de Geología, Area Geodinámica, Universidad de Salamanca. Facultad de Ciencias, Salamanca 37008, Spain. (puy@gugu.usal.es)

M. Beckholmen and C. Juhlin, Department of Earth Sciences, Uppsala University, Villavagen 16, S-75236, Sweden. (mb@geofys.uu.se; cj@geofys.uu.se)

M. Bliznetsov and A. Rybalka, Bazhenov Geophysical Expedition, UralGeolKom, Scheelit, Sverdlovsk District, 624051, Russia.

D. Brown, Instituto de Ciencias de la Tierra 'Jaume Almera', Lluis Solé i Sabaris s/n, Barcelona 08028, Spain. (dbrown@ija.csic.es)

A. Glushkov, UralGeolKom, Urals Geological Survey Expedition, Saldinskaya Partia 448, Ul. Vainera 55, Ekaterinburg, 620000, Russia.

R. Pechnig, Applied Geophysics, Aachen University of Technology, D-52056 Aachen, Germany.

L. Pevzner and R. Pevzner, Nedra, Svoboda str.8/3, 150000, Russia.

(Received July 27, 1999; revised February 21, 2000;
accepted April 12, 2000.)